

Sparse-RS: a versatile framework for query-efficient sparse black-box adversarial attacks

Francesco Croce
University of Tübingen

Maksym Andriushchenko
EPFL

Naman D. Singh
University of Tübingen

Nicolas Flammarion
EPFL

Matthias Hein
University of Tübingen

Abstract

*Sparse adversarial perturbations received much less attention in the literature compared to l_2 - and l_∞ -attacks. However, it is equally important to accurately assess the robustness of a model against sparse perturbations. Motivated by this goal, we propose a versatile framework based on random search, *Sparse-RS*, for score-based sparse targeted and untargeted attacks in the black-box setting. *Sparse-RS* does not rely on substitute models and achieves state-of-the-art success rate and query efficiency for multiple sparse attack models: l_0 -bounded perturbations, adversarial patches, and adversarial frames. Unlike existing methods, the l_0 -version of untargeted *Sparse-RS* achieves almost 100% success rate on ImageNet by perturbing only 0.1% of the total number of pixels, outperforming all existing white-box attacks including l_0 -PGD. Moreover, our untargeted *Sparse-RS* achieves very high success rates even for the challenging settings of 20×20 adversarial patches and 2-pixel wide adversarial frames for 224×224 images. Finally, we show that *Sparse-RS* can be applied for universal adversarial patches where it significantly outperforms transfer-based approaches. The code of our framework is available at <https://github.com/fra31/sparse-rs>.*

1. Introduction

The discovery of the vulnerability of neural networks to adversarial examples [9, 52] revealed that the decision of a classifier or a detector can be changed by small, carefully chosen perturbations of the input. Many efforts have been put into developing increasingly more sophisticated attacks to craft small, semantics-preserving modifications which are able to fool classifiers and bypass many defense mecha-

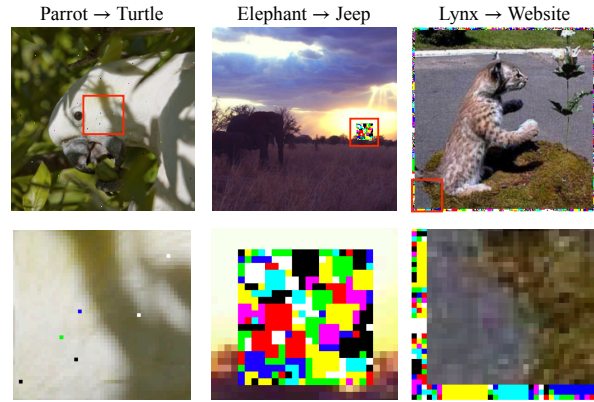


Figure 1. Adversarial examples for sparse threat models (l_0 -bounded, patches, frames) generated with our black-box *Sparse-RS* framework which, unlike existing approaches, does not require surrogate models and is much more query efficient.

nisms [13, 7]. This is typically achieved by constraining or minimizing the l_p -norm of the perturbations, usually either l_∞ [52, 32, 13, 37, 18], l_2 [40, 13, 48, 18] or l_1 [14, 39, 18]. Metrics other than l_p -norms which are more aligned to human perception have been also recently used, e.g. Wasserstein distance [56, 25] or neural-network based ones such as LPIPS [60, 33]. All these attacks have in common the tendency to modify all the elements of the input.

Conversely, *sparse attacks* pursue an opposite strategy: they perturb only a small portion of the original input but possibly with large modifications. Thus, the perturbations are indeed visible but do not alter the semantic content, and can even be applied in the physical world [34, 53, 35]. Sparse attacks include l_0 -attacks [41, 13, 42, 49, 17, 44], adversarial patches [11, 31, 34] and frames [59], where the perturbations have some predetermined structure. Moreover, sparse attacks generalize to tasks outside computer vision, such as malware detection or natural language pro-

cessing, where the nature of the domain imposes to modify only a limited number of input features [23, 30].

We here focus on the black-box score-based scenario, where the attacker can only access the predicted scores of a classifier f , but does not know the network weights and in particular cannot use gradients of f wrt the input (as in the white-box setup). We do not consider more restrictive (e.g., decision-based attacks [10, 12] where the adversary only knows the label assigned to each input) or more permissive (e.g., a surrogate model similar to the victim one is available [15, 27]) cases. For the l_0 -threat models only a few black-box attacks exist [41, 49, 17, 61], and only [57] focuses on query efficiency and scales to datasets like ImageNet without suffering from prohibitive computational cost. For adversarial patches and frames, black-box methods are mostly limited to transfer attacks, that is a white-box attack is performed on a surrogate model, with the exception of [57] who use a predefined dictionary of patches.

Contributions. We propose *Sparse-RS*, a simple and flexible framework based on random search to efficiently generate sparse adversarial examples in the black-box score-based setting. Our framework is effective with minimal adaptations for various sparse threat models. First, we show the superior performance of *Sparse-RS* adapted to the l_0 -threat model—which we call l_0 -RS—in terms of success rate and query efficiency compared to existing black-box attacks in a variety of settings. Moreover, l_0 -RS achieves better results than white-box attacks on both standard and robust models and thus is particularly valuable to accurately evaluate adversarial robustness. Second, within our *Sparse-RS* framework, we introduce *Patch-RS* and *Frame-RS*, for adversarial patches and frames: both outperform in terms of success rate and query efficiency existing competitors and black-box adaptations of projected gradient descent (PGD) attacks via gradient estimation. Finally, we craft universal patch attacks without relying on a surrogate model like all other current black-box attacks. We visualize the adversarial examples generated by *Sparse-RS* for all threat models in Fig. 1.

2. Black-box adversarial attacks

Let $f : \mathcal{S} \subseteq \mathbb{R}^d \rightarrow \mathbb{R}^K$ be a classifier which assigns input $x \in \mathcal{S}$ to class $y = \arg \max_{r=1, \dots, K} f_r(x)$. The goal of an *untargeted* attack is to craft a perturbation $\delta \in \mathbb{R}^d$ such that

$$\arg \max_{r=1, \dots, K} f_r(x + \delta) \neq y, \quad x + \delta \in \mathcal{S} \quad \text{and} \quad \delta \in \mathcal{T},$$

where \mathcal{S} is the input domain and \mathcal{T} are the constraints the adversarial perturbation has to fulfill (e.g. bounded l_p -norm), while a *targeted* attack aims at finding δ such that

$$\arg \max_{r=1, \dots, K} f_r(x + \delta) = t, \quad x + \delta \in \mathcal{S} \quad \text{and} \quad \delta \in \mathcal{T},$$

with t as target class. Generating such δ can be translated into an optimization problem as

$$\min_{\delta \in \mathbb{R}^d} L(f(x + \delta), t) \quad \text{s.t.} \quad x + \delta \in \mathcal{S} \quad \text{and} \quad \delta \in \mathcal{T} \quad (1)$$

by choosing a label t and loss function L whose minimization leads to the desired classification. By *threat model* we mean the overall attack setting determined by the goal of the attacker (targeted vs untargeted attack), the level of knowledge (white- vs black-box), and the perturbation set \mathcal{T} .

Many algorithms have been proposed to solve Problem (1) in the black-box setting where one cannot use gradient-based methods. One of the first approaches is [21] where they propose to sample candidate adversarial occlusions via the Metropolis MCMC method, which can be seen as a way to generate adversarial patches whose content is not optimized. [28, 55] propose to approximate the gradient through finite difference methods, later improved to reduce their high computational cost in terms of queries of the victim models [8, 54, 29]. Alternatively, [3, 36] use genetic algorithms in the context of image classification and malware detection respectively. A line of research has focused on rephrasing l_∞ -attacks as discrete optimization problems [50, 2, 38], where specific techniques lead to significantly better query efficiency. [24] adopt a variant of random search to produce perturbations with a small l_2 -norm.

The method closest in spirit to our proposed framework is the Square Attack of [4], which is state-of-the-art for l_∞ - and l_2 -bounded black-box attacks. It uses random search to iteratively generate samples on the surface of the l_∞ - or l_2 -balls. This, together with a carefully crafted sampling distribution that relies on square-shaped updates and specific initialization, leads to a simple algorithm which outperforms more sophisticated attacks in terms of success rate and query efficiency. In this paper we show that the random search idea can be generalized to the case of sparse attacks, where the non-convex, combinatorial constraints are not easily handled even by gradient-based *white-box* attacks.

3. Sparse-RS: a random search based framework for adversarial attacks

Random search (RS) is a well known scheme for derivative free optimization [46]. Given an objective function L to minimize, a starting point $x^{(0)}$ and a sampling distribution \mathcal{D} , an iteration of RS at step i is given by

$$\delta \sim \mathcal{D}(x^{(i)}), \quad x^{(i+1)} = \arg \min_{y \in \{x^{(i)}, x^{(i)} + \delta\}} L(y). \quad (2)$$

At every step an update of the current iterate $x^{(i)}$ is sampled according to \mathcal{D} and accepted only if it decreases the objective value, otherwise the procedure is repeated. Although not explicitly mentioned in Eq. (2), constraints on the iterates $x^{(i)}$ can be integrated by ensuring that δ is sampled

Algorithm 1: Sparse-RS

input : loss L , input x_{orig} , max query N , sparsity k ,
input space constraints \mathcal{S}
output: approximate minimizer of L

- 1 $M \leftarrow k$ indices of elements to be perturbed
- 2 $\Delta \leftarrow$ values of the perturbation to be applied
- 3 $z \leftarrow x_{\text{orig}}, z_M \leftarrow \Delta$ // set elements in M to values in Δ
- 4 $L^* \leftarrow L(z), i \leftarrow 0$ // initialize loss
- 5 **while** $i < N$ **and** *success not achieved* **do**
- 6 $M' \leftarrow$ sampled modification of M
 // new set of indices
- 7 $\Delta' \leftarrow$ sampled modification of Δ
 // new perturbation
- 8 $z \leftarrow x_{\text{orig}}, z_{M'} \leftarrow \Delta'$
 // create new candidate in \mathcal{S}
- 9 **if** $L(z) < L^*$ **then**
- 10 $L^* \leftarrow L(z), M \leftarrow M', \Delta \leftarrow \Delta'$ // if
 loss improves, update sets
- 11 $i \leftarrow i + 1$
- 12 $z \leftarrow x_{\text{orig}}, z_M \leftarrow \Delta$ // return best Δ
- 13 **return** z

so that $x^{(i)} + \delta$ is a feasible solution. Thus even complex, e.g. combinatorial, constraints can easily be integrated as RS just needs to be able to produce feasible points in contrast to gradient-based methods which depend on a continuous set to optimize over. While simple and flexible, RS is an effective tool in many tasks [58, 4], with the key ingredient for its success being a task-specific sampling distribution \mathcal{D} to guide the exploration of the space of possible solutions.

We summarize our general framework based on random search to generate sparse adversarial attacks, Sparse-RS, in Alg. 1, where the sparsity k indicates the maximum number of features that can be perturbed. A sparse attack is characterized by two variables: the set of components to be perturbed M and the values Δ to be inserted at M to form the adversarial input. To optimize over both of them we first sample a random update of the locations M of the current perturbation (step 6) and then a random update of its values Δ (step 7). In some threat models (e.g. adversarial frames) the set M cannot be changed, so $M' \equiv M$ at every step. How Δ' is generated depends on the specific case, so we present the individual procedures in the next sections.

Common to all variants of Sparse-RS is that the whole budget for the perturbations is fully exploited both in terms of number of modified components and magnitude of the elementwise changes (constrained only by the limits of the input domain \mathcal{S}). This follows the intuition that larger perturbations should lead faster to an adversarial example. Moreover, the difference of the candidates M' and Δ' with M

and Δ shrinks gradually with the iterations which mimics the reduction of the step size in gradient-based optimization: initial large steps allow to quickly decrease the objective loss, but smaller steps are necessary to refine a close-to-optimal solution at the end of the algorithm. Finally, we impose a limit N on the maximum number of queries of the classifier, i.e. evaluations of the objective function.

As objective function L to be minimized, we use in the case of untargeted attacks the margin loss $L_{\text{margin}}(f(\cdot), y) = f_y(\cdot) - \max_{r \neq y} f_r(\cdot)$, where y is the correct class, so that $L < 0$ is equivalent to misclassification, whereas for targeted attacks we use the cross-entropy loss L_{CE} of the target class t , namely $L_{\text{CE}}(f(\cdot), t) = -f_t(\cdot) + \log \left(\sum_{r=1}^K e^{f_r(\cdot)} \right)$.

4. Sparse-RS for l_0 -bounded attacks

The first threat model we consider is l_0 -bounded adversarial examples where only k pixels of an input $x_{\text{orig}} \in [0, 1]^{h \times w \times c}$ (width w , height h , color c) can be modified, but there are no constraints on the magnitude of the perturbations except for those of the input domain.

l_0 -RS algorithm. Let U be the set of the $h \cdot w$ pixels. In this case the set $M \subset U$ from Alg. 1 is initialized sampling uniformly k elements of U , while $\Delta \sim \mathcal{U}(\{0, 1\}^{k \times c})$, that is random values in $\{0, 1\}$ (every perturbed pixel gets one of the corners of the color cube $[0, 1]^c$). Then, at the i -th iteration, we randomly select $A \subset M$ and $B \subset U \setminus M$, with $|A| = |B| = \alpha^{(i)} \cdot k$, and create $M' = (M \setminus A) \cup B$. Δ' is formed by sampling random values from $\{0, 1\}^c$ for the elements in B , i.e. those which were not perturbed at the previous iteration. The quantity $\alpha^{(i)}$ controls how much M' differs from M and decays following a predetermined piecewise constant schedule rescaled according to the maximum number of queries N . The schedule is completely determined by the single value α_{init} , used to calculate $\alpha^{(i)}$ for every iteration i , which is also the only free hyperparameter of our scheme (details about the algorithm, schedule and values of α_{init} in App. A and B).

4.1. Theoretical analysis of l_0 -RS

We here analyze l_0 -RS for a binary classifier. While the analysis does not directly transfer to neural networks, most modern neural network architectures result in piecewise linear classifiers [5, 16], so that the result approximately holds in a sufficiently small neighborhood of the target point x .

As in the malware detection task from Sec. 4.4, we assume that the input x has binary features, $x \in \{0, 1\}^d$, and we denote the label by $y \in \{-1, 1\}$ and the gradient of the linear model by $w_x \in \mathbb{R}^d$. Then the Problem (1) of finding

the optimal l_0 adversarial example is equivalent to:

$$\begin{aligned} \arg \min_{\substack{\|\delta\|_0 \leq k \\ x_i + \delta_i \in \{0,1\}}} y \langle w_x, x + \delta \rangle &= \arg \min_{\substack{\|\delta\|_0 \leq k \\ \delta_i \in \{0,1-2x_i\}}} \langle yw_x, \delta \rangle \\ &= \arg \min_{\substack{\|\delta\|_0 \leq k \\ \delta_i \in \{0,1\}}} \underbrace{\langle yw_x \odot (1-2x), \delta \rangle}_{\hat{w}_x}, \end{aligned}$$

where \odot denotes the elementwise product. In the white-box case, i.e. when w_x is known, the solution is to simply set $\delta_i = 1$ for the k smallest weights of \hat{w}_x . The black-box case, where w_x is unknown and we are only allowed to query the model predictions $\langle \hat{w}_x, z \rangle$ for any $z \in \mathbb{R}^d$, is more complicated since the naive weight estimation algorithm requires $O(d)$ queries to first estimate \hat{w}_x and then to perform the attack by selecting the k minimal weights. This naive approach is prohibitively expensive for high-dimensional datasets (e.g., $d = 150,528$ on ImageNet assuming $224 \times 224 \times 3$ images). However, the problem of generating adversarial examples does not have to be always solved exactly, and often it is enough to find an approximate solution. Therefore we can be satisfied with only identifying k among the m smallest weights. Indeed, the focus is not on exactly identifying the solution but rather on having an algorithm that in expectation requires a *sublinear* number of queries. With this goal, we show that l_0 -RS satisfies this requirement for large enough m .

Proposition 4.1 *The expected number t_k of queries needed for l_0 -RS with $\alpha^{(i)} = 1/k$ to find a set of k weights out of the smallest m weights of a linear model is:*

$$\mathbb{E}[t_k] = (d-k)k \sum_{i=0}^{k-1} \frac{1}{(k-i)(m-i)} < (d-k)k \frac{\ln(k) + 2}{m-k}.$$

The proof is deferred to App. F and resembles that of the coupon collector problem [22]. For non-linear models, l_0 -RS uses $\alpha^{(i)} > 1/k$ for better exploration initially, but then progressively reduces it. The main conclusion from Proposition 4.1 is that $\mathbb{E}[t_k]$ becomes sublinear for large enough gap $m-k$, as we illustrate in Fig. 10 in the Appendix.

4.2. Query efficiency of l_0 -RS compared to other black-box attacks

We compare l_0 -RS to other black-box untargeted attacks in terms of success rate versus query efficiency. The results of targeted attacks can be found in App. A. Here we focus on attacking normally trained VGG-16-BN and ResNet-50 models on ImageNet, which contains RGB images resized to shape 224×224 , that is 50,176 pixels, belonging to 1,000 classes. We consider perturbations of size $k \in \{50, 150\}$ pixels to assess the effectiveness of the untargeted attacks at different thresholds with a limit of 10,000 queries. We

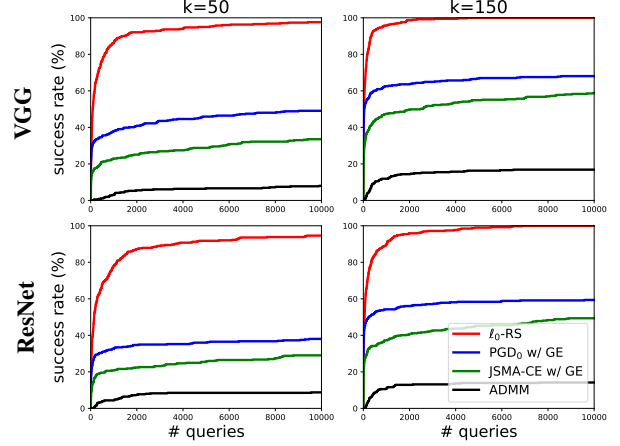


Figure 2. Progression of the success rate vs number of queries for black-box untargeted l_0 -attacks on ImageNet. At all sparsity levels l_0 -RS (red) outperforms PGD₀ (blue) and JSMA-CE (green) with gradient estimation and ADMM attack [61] (black).

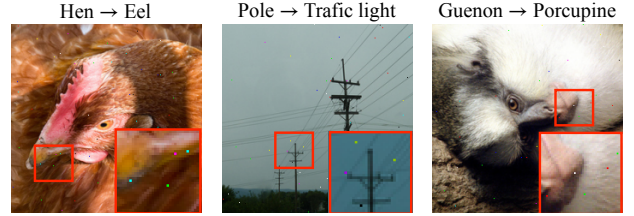


Figure 3. Untargeted l_0 adversarial examples generated by our l_0 -RS algorithm for $k = 50$ pixels.

evaluate the success rate on the initially correctly classified points out of 500 images from the validation set.

Competitors. Many existing black-box l_0 -attacks [41, 49, 17] do not aim at query efficiency against norm-bounded perturbations, and rather try to minimize the size of the perturbations. Among them, only CornerSearch [17] and ADMM attack [61] scale to ImageNet. However, CornerSearch requires $8 \times \#pixels$ queries only for the initial phase, exceeding the query limit we fix by more than 40 times. The ADMM attack [61] tries to achieve a successful perturbation and then reduces its norm and is applicable at ImageNet scale. Moreover, we introduce black-box versions of PGD₀ [17] with the gradient estimated by finite difference approximation as done in many prior works (e.g., see [28]). We also introduce, to set a strong baseline, JSMA-CE which is a version of the JSMA algorithm [42] that we adapt to the black-box setting: (1) to make it more query efficient, we estimate the gradient of the cross-entropy loss instead of gradients of *each* class logit, (2) on each iteration, we modify the *pixels* (instead of subpixel values) with the highest gradient contribution. We provide more details about the attacks in App. A.

Results. We show in Fig. 2 the progression of the success rate vs the number of queries for all black-box attacks.

attack	type	$k = 50$ (pixels)	
		VGG	ResNet
SAPF* [20]	white-box	16.0%	13.0%
ProxLogBarrier [44]	white-box	37.8%	33.2%
JSMA-CE [42]	white-box	42.6%	39.6%
SparseFool [39]	white-box	63.6%	66.0%
PGD ₀ [17]	white-box	87.0%	81.2%
ADMM attack [61]	black-box	30.3%	29.0%
JSMA-CE with GE	black-box	49.6%	44.8%
PGD ₀ [17] with GE	black-box	61.4%	51.8%
CornerSearch* [17]	black-box	82.0%	72.0%
l_0 -RS	black-box	98.2%	95.8%

Table 1. Robust test error of untargeted l_0 -attacks on ImageNet with a l_0 -budget of 50 pixels. The entries with * are evaluated on 100 points instead of 500 because of their high computational cost. All black-box attacks use 10k queries except CornerSearch which uses 600k. l_0 -RS outperforms all black- and white-box attacks.

In all cases, l_0 -RS outperforms its competitors in terms of the final success rate by a large margin—the second best method (PGD₀ w/ GE) is at least 30% worse. Moreover, l_0 -RS is query efficient as it achieves results close to the final ones already with a low number of queries. For example, on VGG with $k = 150$, l_0 -RS achieves 100% of success rate using on average only 171 queries, with a median of 25. We also note that unlike other methods, l_0 -RS can achieve almost 100% success rate by perturbing 50 pixels which is *only* 0.1% of the total number of pixels. We visualize the resulting adversarial examples of l_0 -RS in Fig. 3.

4.3. Using l_0 -RS for accurate robustness evaluation

In this section, our focus is the accurate evaluation of robustness in the l_0 -threat model. For this, we evaluate existing white-box methods and black-box methods together. Instead of the success rate taken only over correctly classified examples, here we rather consider *robust error* (similarly to [37]), which is defined as the classification error on the adversarial examples crafted by an attacker.

White-box attacks on ImageNet. We test the robustness of the ImageNet models introduced in the previous section to perturbations of at most $k = 50$ pixels. We evaluate multiple existing white-box attacks: SAPF [20], ProxLogBarrier [44], and SparseFool [39]. However, these methods aim to optimize directly the l_0 -norm with respect to the input *features (channels)*, and not *pixels* as in our threat model. As every pixel has three channels we thus give them the advantage of using $k = 150$ as in this case our pixel-based threat model is a subset of their feature-based threat model. We also evaluate two white-box baselines that do take into account the pixel-structure of the image inputs: PGD₀ introduced in [17], and JSMA-CE proposed in [42] where we use the gradient of the cross-entropy loss to generate the saliency map. Moreover, we show the results of

attack	type	$k = 12$ (pixels)	
		ABS	Binary ABS
Pointwise Attack [49]	black-box	31%	23%
CornerSearch [17]	black-box	29%	28%
l_0 -RS	black-box	55%	51%

Table 2. Robust test error obtained on the robust generative models of [49] on MNIST by different attacks on 100 test points.

the black-box attacks from the previous section (all with a query limit of 10,000), and additionally use the black-box CornerSearch [17] for which we use a query limit of 600k and which is thus only partially comparable. Details of the attacks are available in App. A. Table 1 shows the robust error given by all competitors: l_0 -RS achieves the best results on both VGG and ResNet, outperforming black- and white-box attacks. We note that while the PGD attack has been observed to give accurate robustness estimates for l_∞ - and l_2 -norms [37], this is not the case for the l_0 constraint set. This is due to the discrete structure of the l_0 -ball which is not amenable for continuous optimization.

Robust generative models on MNIST. Schott et al. [49] propose two robust generative models on MNIST: ABS and Binary ABS, which showed high robustness against multiple types of l_p -bounded adversarial examples. These two classifiers rely on optimization-based inference using a variational auto-encoder (VAE) with 50 steps of gradient descent for each prediction (times 1,000 repetitions). It is too expensive to get gradients with respect to the input through the optimization process, thus [49] evaluate only black-box attacks. [49] test l_0 -robustness with sparsity $k = 12$ using their proposed Pointwise Attack with 10 restarts. As an additional baseline, we evaluate CornerSearch [17] with a budget of 50,000 queries as it performs better than PGD₀ with gradient estimation. We compare these two methods to l_0 -RS with an equivalent budget of 10,000 queries and 5 random restarts. Table 2 summarizes the robust test error (on 100 points) achieved by the attacks (the results of Pointwise Attack are taken from [49]). For both models, l_0 -RS yields the strongest evaluation of robustness suggesting that the ABS models are less robust than previously believed. This illustrates that despite we have *full access* to the attacked VAE model, a strong *black-box* l_0 -attack can still be useful for an accurate robustness evaluation.

4.4. l_0 -RS beyond image classification

Finally, we apply our attack l_0 -RS in a different domain, showing its versatility. We consider the Drebin dataset [6] consisting of 129,013 benign and malicious Android apps, with $d = 545,333$ features. An app is encoded as a binary vector $x \in \{0, 1\}^d$ indicating whether a feature is present or not in x (unlike image classification the input space is in this case discrete). We apply l_0 -RS as described for images

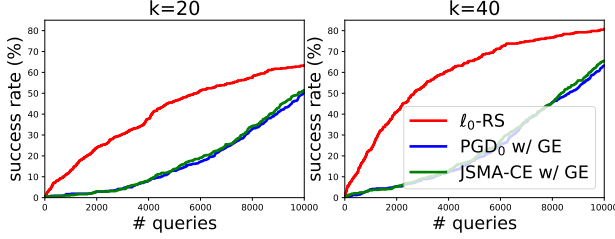


Figure 4. Success rate vs number of queries in fooling a malware detector for sparsity levels $k \in \{20, 40\}$. l_0 -RS outperforms the competitors, with a large gap in the low query regime.

as input by setting $h = d$ and $w = c = 1$ such that $x \in \{0, 1\}^{d \times 1 \times 1}$ (details in App. B). Following [23], we allow the attacks to only add features so that the functionality of the apps is preserved (no features are removed). We train a fully connected model for malware detection which has a test accuracy of 98.85% and test its robustness by trying to modify 500 malicious apps from the test set so that they are detected as benign, modifying $k \in \{20, 40\}$ features, with a maximum of 10,000 queries.

Competitors. [23] successfully fooled similar models with a variant of the white-box JSMA [42], and [43] confirms that it is the most effective technique on Drebin, compared to the attacks of [51, 1, 26] including adaptation of FGSM [52] and PGD [32, 37]. We use JSMA [42, 23] and PGD₀ [17] in a black-box version with gradient estimation (details in App. B). [36] propose a black-box genetic algorithm with prior knowledge of the importance of the features for misclassification (via a pretrained random forest) which is not comparable to our threat model.

Results. Fig. 4 shows the progression of success rate (computed on the initially correctly classified apps) of the attacks over number of queries used. At both sparsity levels, our l_0 -RS attack (in red) outperforms JSMA (green) and PGD₀ (blue), especially in the low query regime.

5. Sparse-RS for adversarial patches

Another type of sparse attacks which recently received attention are adversarial patches introduced by [11]. There the perturbed pixels are localized, often square-shaped, and limited to a small portion of the image but can be changed in an arbitrary way. While some works [11, 31] aim at universal patches, which fool the classifier regardless of the image and the position where they are applied, which we consider in Sec. 7, we focus first on image-specific patches as in [57, 45] where one optimizes both the content and the location of the patch for each image independently.

General algorithm for patches. Note that both location (step 6 in Alg. 1) and content (step 7 in Alg. 1) have to be optimized in Sparse-RS, and on each iteration we check only one of these updates. We test the effect of different frequencies of location/patch updates in an ablation

study in App. G.2. Since the location of the patch is a discrete variable, random search is particularly well suited for its optimization. For the location updates in step 6 in Alg. 1, we randomly sample a new location in a 2D l_∞ -ball around the current patch position (using clipping so that the patch is fully contained in the image). The radius of this l_∞ -ball shrinks with increasing iterations in order to perform progressively more local optimization (see App. C for details).

For the update of the patch itself in step 7 in Alg. 1, the only constraints are given by the input domain $[0, 1]^d$. Thus in principle any black-box method for an l_∞ -threat model can be plugged in there. We use Square Attack (SA) [4] and SignHunter (SH) [2] as they represent the state-of-the-art in terms of success rate and query efficiency. We integrate both of them in our Sparse-RS framework and refer to them as Sparse-RS + SH and Sparse-RS + SA. Next we propose a novel random search based attack motivated by SA which together with our location update yields our novel Patch-RS attack.

Patch-RS. While SA and SH are state-of-the-art for l_∞ -attacks, they have been optimized for rather small perturbations whereas for patches all pixels can be manipulated arbitrarily in $[0, 1]$. Here, we design an initialization scheme and a sampling distribution specific for adversarial patches. As initialization (step 2 of Alg. 1), Patch-RS uses randomly placed squares with colors in $\{0, 1\}^3$, then it samples updates of the patch (step 7) with shape of squares, of size decreasing according to a piecewise constant schedule, until a refinement phase in the last iterations, when it performs single-channel updates (exact schedule in App. C). This is in contrast to SA where random vertical stripes are used as initialization and always updates for all three channels of a pixel are sampled. The ablation study in App. G.2 shows how both modifications contribute to the improved performance of Patch-RS.

Experiments. In addition to Sparse-RS + SH, Sparse-RS + SA, and Patch-RS, we consider two existing methods. i) TPA [57] which is a black-box attack aiming to produce image-specific adv. patches based on reinforcement learning. While [57] allows multiple patches for an image, we use TPA in the standard setting of a single patch. ii) Location-Optimized Adversarial Patches (LOAP) [45], a white-box attack that uses PGD for the patch updates, which we combine with gradient estimation in order to use it in the black-box scenario (see App. C for details). In Table 3 we report success rate, mean and median number of queries used for untargeted attacks with patch size 20×20 and query limit of 10,000 and for targeted attacks (random target class for each image) with patch size 40×40 and maximally 50,000 queries. We attack 500 images of ImageNet with VGG and ResNet as target models. The query statistics are computed on *all* 500 images, i.e. without restricting to only successful adversarial examples, as this makes the

		attack	VGG			ResNet		
			success rate	mean queries	med. queries	success rate	mean queries	med. queries
untargeted.	black-box	LOAP [45] w/ GE	55.1% \pm 0.6	5879 \pm 51	7230 \pm 377	40.6% \pm 0.1	6870 \pm 10	10000 \pm 0
		TPA [57]	46.1% \pm 1.1	6085* \pm 83	8080* \pm 1246	49.0% \pm 1.2	5722* \pm 64	5280* \pm 593
		Sparse-RS + SH [2]	82.6%	2479	514	75.3%	3290	549
		Sparse-RS + SA [4]	85.6% \pm 1.1	2367 \pm 83	533 \pm 40	78.5% \pm 1.0	2877 \pm 64	458 \pm 43
		Patch-RS	87.8% \pm 0.7	2160 \pm 44	429 \pm 22	79.5% \pm 1.4	2808 \pm 89	438 \pm 68
		White-box LOAP [45]	98.3%	-	-	82.2%	-	-
targeted	black-box	LOAP [45] w/ GE	23.9% \pm 0.9	44134 \pm 71	50000 \pm 0	18.4% \pm 0.9	45370 \pm 88	50000 \pm 0
		TPA [57]	5.1% \pm 1.2	29934* \pm 462	34000* \pm 0	6.0% \pm 0.5	31690* \pm 494	34667* \pm 577
		Sparse-RS + SH [2]	63.6%	25634	19026	48.6%	31250	50000
		Sparse-RS + SA [4]	70.9% \pm 1.2	23749 \pm 346	15569 \pm 568	53.7% \pm 0.9	32290 \pm 239	40122 \pm 2038
		Patch-RS	72.7% \pm 0.9	22912 \pm 207	14407 \pm 866	55.6% \pm 1.5	30290 \pm 317	34775 \pm 2660
		White-box LOAP [45]	99.4%	-	-	94.8%	-	-

Table 3. Success rate and query statistics of image-specific patches. Black-box attacks are given 10k/50k queries for untargeted/targeted case. SH [2] is a deterministic method. The query statistics are computed on *all* images with 5 random seeds. * TPA uses an early stopping mechanism to save queries, thus might not use all queries. Patch-RS outperforms all other methods in success rate and query efficiency.

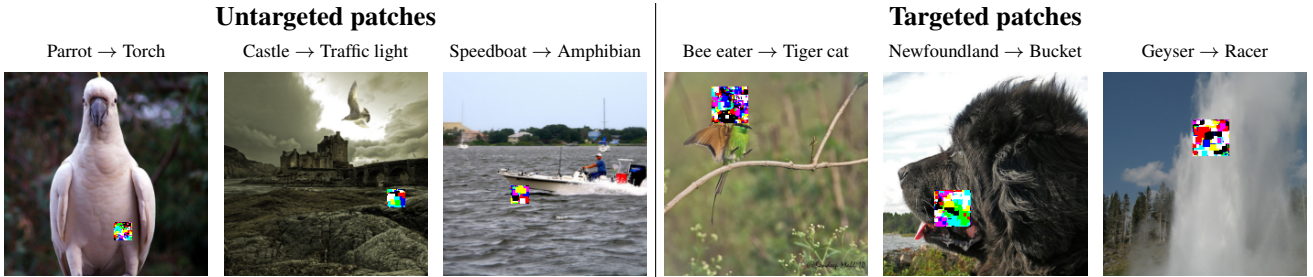


Figure 5. Image-specific untargeted (20×20 pixels) and targeted (40×40 pixels) patches generated by our Patch-RS algorithm.

query efficiency comparable for different success rates. Our Sparse-RS + SH, Sparse-RS + SA and Patch-RS outperform existing methods by a large margin, showing the effectiveness of our scheme to optimize both location and patch. Among them, our specifically designed Patch-RS achieves the best results in all metrics. We visualize its resulting adversarial examples in Fig. 5.

6. Sparse-RS for adversarial frames

Adversarial frames introduced in [59] are another sparse threat model where the attacker is allowed to perturb only pixels along the borders of the image. In this way, the total number of pixels available for the attack is small (3%-5% in our experiments), and in particular the semantic content of the image is not altered by covering features of the correct class. Thus, this threat model shows how even peripheral changes can influence the classification decision.

General algorithm for frames. Unlike patches (Sec. 5), for frames the set of pixels M which can be perturbed (see Alg. 1) is fixed. However, similarly to patches, the pixels of the frame can be changed arbitrarily in $[0, 1]^3$ and thus we can use l_∞ -black-box attacks for step 7 in Alg. 1 which we denote as Sparse-RS + SH and Sparse-RS + SA.

While SH is agnostic to the shape of the perturbations defined by adversarial frames and can be successfully applied for step 7 without further modifications, Sparse-RS + SA leads to suboptimal performance (see Table 4). Indeed, in the frame setting, the sampling distribution of SA requires its square updates to be entirely contained in the frame which due to its small width strongly limits the potential updates. Thus, to achieve better performance, we propose a new sampling distribution specific to frames which, combined with Sparse-RS framework, we call Frame-RS.

Frame-RS algorithm. Our new sampling distribution (used for step 7 of Alg. 1) returns squares that only *partially* overlap with the frame. Effectively, we have more flexible updates, often of non-squared shape. Moreover, similarly to Patch-RS, we introduce single-channel updates in the final phase. We also use a different initialization in step 2: uniformly random sampling instead of vertical stripes. As a result, Frame-RS shows significantly better results than both Sparse-RS + SH and Sparse-RS + SA.

Experiments. As a baseline, we use the Adversarial Framing (AF) method of [59] applied to image-specific frames (1) in the white-box setting and (2) in the black-box setting where we perform PGD with gradient estimation. For untargeted attacks we use frames of width 2 and a

		attack	VGG			ResNet		
			success rate	mean queries	med. queries	success rate	mean queries	med. queries
untarget.	(2 px wide)	black-box AF [59] w/ GE	57.6% \pm 0.4	5599 \pm 23	6747 \pm 127	70.6% \pm 0.7	4568 \pm 13	3003 \pm 116
		Sparse-RS + SH [2]	79.9%	3169	882	88.7%	2810	964
		Sparse-RS + SA [4]	77.8% \pm 2.0	3391 \pm 215	1292 \pm 220	80.7% \pm 1.4	3073 \pm 111	1039 \pm 93
		Frame-RS	90.2% \pm 0.3	2366 \pm 26	763 \pm 32	94.0% \pm 0.3	1992 \pm 34	588 \pm 10
		White-box AF [59]	100%	-	-	100%	-	-
targeted	(3 px wide)	black-box AF [59] w/ GE	16.1% \pm 1.5	45536 \pm 328	50000 \pm 0	40.6% \pm 1.4	39753 \pm 459	50000 \pm 0
		Sparse-RS + SH [2]	52.0%	32223	41699	73.2%	25929	20998
		Sparse-RS + SA [4]	32.9% \pm 1.9	38463 \pm 870	50000 \pm 0	47.5% \pm 2.8	33321 \pm 980	48439 \pm 3500
		Frame-RS	65.7% \pm 0.4	28182 \pm 99	27590 \pm 580	88.0% \pm 0.9	19828 \pm 130	15325 \pm 370
		White-box AF [59]	100%	-	-	100%	-	-

Table 4. Success rate and query statistics of image-specific frames computed for 5 seeds. Black-box attacks are given 10k/50k queries for untargeted/targeted case. SH [2] is a deterministic method. Frame-RS achieves the best success rate and efficiency in all settings.

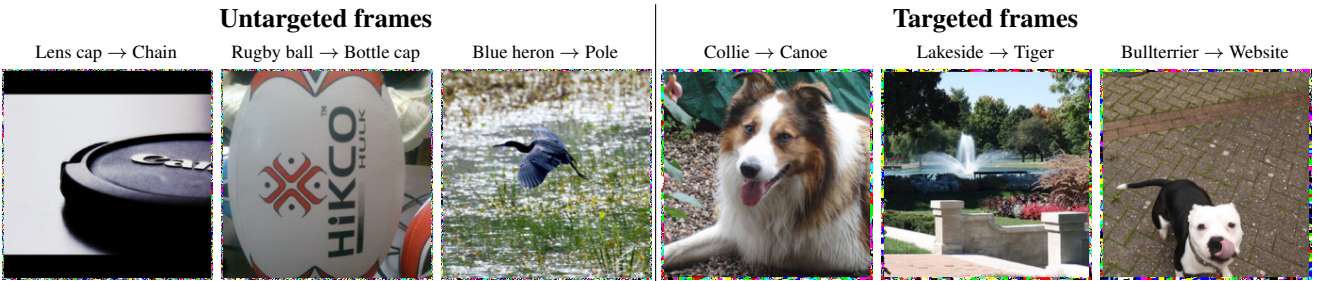


Figure 6. Image-specific untargeted (2 pixel wide) and targeted (3 pixel wide) frames generated by our Frame-RS algorithm.

maximum of 10,000 queries, and for targeted attacks we use frames of width 3 and maximally 50,000 queries. In Table 4 we show that our Frame-RS achieves the best success rate (at least 10% higher than the closest competitor) and much better query efficiency in all settings. In particular, Frame-RS significantly outperforms Sparse-RS + SA, showing that our new sampling distribution is crucial to obtain an effective attack. For the untargeted case the success rate of our black-box Frame-RS is close to that of the white-box AF method which achieves 100% success rate. We visualize the resulting adversarial examples in Fig. 6.

7. Universal adversarial patches

A challenging threat model is that of a black-box, targeted universal adversarial patch attack where the classifier should be fooled into a chosen target class when the patch is applied inside any image of some other class. Previous works rely on transfer attacks: in [11] the universal patch is created using a white-box attack on surrogate models, while the white-box attack of [31] directly optimizes the patch for the target model on a set of training images and then only tests generalization to unseen images. Our goal is a targeted black-box attack which crafts universal patches that generalize to unseen images when applied at random locations. To the best of our knowledge, this is the first method for this threat model which does not rely on a surrogate model.

We employ Alg. 1 where for the creation of the patches in step 7 we use either SH, SA or our novel sampling distribution introduced in Patch-RS in Sec. 5. The loss in Alg. 1 is computed on a small batch of 30 training images and the initial locations M of the patch in each of the training images are sampled randomly. In order not to overfit on the set of training batch, we resample both training images and locations of the patches (step 6 in Alg. 1) every 10k queries, where our total query budget is 100k. Similar to stochastic gradient descent this can be seen as stochastic optimization of the population loss (expectation over images and locations) via random search.

Experiments. We use Sparse-RS + SH/SA and Patch-RS with the above optimization scheme to design universal patches of size 50×50 for 10 random target classes on VGG and ResNet (we repeat it for 3 random seeds for random search based methods). We compare to the transfer based attacks obtained via white-box PGD [37] and MI-FGSM [19] using the other network as surrogate model. The results in Table 5 show that our Sparse-RS + SH/SA and Patch-RS outperforms transfer-based attacks by large margin.

8. Conclusions

We propose a versatile framework, Sparse-RS, which achieves state-of-the-art success rate and query efficiency

<i>attack</i>	VGG	ResNet
Transfer PGD [37]	3.3%	0.0%
Transfer MI-FGSM [19]	1.3%	0.0%
Sparse-RS + SH [2]	63.9%	13.8%
Sparse-RS + SA [4]	72.9% ± 3.6	29.6% ± 5.6
Patch-RS	70.8% ± 1.3	30.4% ± 8.0

Table 5. Success rate of targeted universal patches of size 50×50 .

in multiple sparse threat models: l_0 -bounded perturbations, image-specific adversarial patches and adversarial frames. Moreover, it is effective in the challenging task of crafting universal adversarial patches without relying on surrogate models, unlike the existing methods. We think that strong black-box adversarial attacks are a very important component to assess the adversarial robustness of classifiers against such localized and structured attacks, which go beyond the standard l_∞ and l_2 threat models.

Acknowledgements

We thank Yang et al. [57] for quickly releasing their code and answering our questions. F.C., N.S. and M.H. acknowledge support from the German Federal Ministry of Education and Research (BMBF) through the Tübingen AI Center (FKZ: 01IS18039A), the DFG Cluster of Excellence “Machine Learning – New Perspectives for Science”, EXC 2064/1, project number 390727645, and by DFG grant 389792660 as part of TRR 248.

References

- [1] A. Al-Dujaili, A. Huang, E. Hemberg, and U.-M. O’Reilly. Adversarial deep learning for robust detection of binary encoded malware. In *IEEE Security and Privacy Workshops (SPW)*, pages 76–82, 2018. 6
- [2] A. Al-Dujaili and U.-M. O’Reilly. There are no bit parts for sign bits in black-box attacks. In *ICLR*, 2020. 2, 6, 7, 8, 9, 15, 16, 17, 18, 22, 23
- [3] M. Alzantot, Y. Sharma, S. Chakraborty, and M. Srivastava. Genattack: practical black-box attacks with gradient-free optimization. *Genetic and Evolutionary Computation Conference (GECCO)*, 2019. 2
- [4] M. Andriushchenko, F. Croce, N. Flammarion, and M. Hein. Square attack: a query-efficient black-box adversarial attack via random search. *ECCV*, 2020. 2, 3, 6, 7, 8, 9, 15, 17, 18, 20, 22, 23
- [5] R. Arora, A. Basuy, P. Mianjyz, and A. Mukherjee. Understanding deep neural networks with rectified linear unit. In *ICLR*, 2018. 3
- [6] D. Arp, M. Spreitzenbarth, M. Hubner, H. Gascon, K. Rieck, and C. Siemens. Drebin: Effective and explainable detection of android malware in your pocket. In *NDSS*, volume 14, pages 23–26, 2014. 5, 14
- [7] A. Athalye, N. Carlini, and D. A. Wagner. Obfuscated gradients give a false sense of security: Circumventing defenses to adversarial examples. In *ICML*, 2018. 1
- [8] A. N. Bhagoji, W. He, B. Li, and D. Song. Practical black-box attacks on deep neural networks using efficient query mechanisms. In *ECCV*, 2018. 2
- [9] B. Biggio, I. Corona, D. Maiorca, B. Nelson, N. Srndic, P. Laskov, G. Giacinto, and F. Roli. Evasion attacks against machine learning at test time. In *ECML/PKDD*, 2013. 1
- [10] W. Brendel, J. Rauber, and M. Bethge. Decision-based adversarial attacks: Reliable attacks against black-box machine learning models. In *ICLR*, 2018. 2
- [11] T. B. Brown, D. Mané, A. Roy, M. Abadi, and J. Gilmer. Adversarial patch. In *NeurIPS 2017 Workshop on Machine Learning and Computer Security*, 2017. 1, 6, 8, 17
- [12] T. Brunner, F. Diehl, M. T. Le, and A. Knoll. Guessing smart: biased sampling for efficient black-box adversarial attacks. *ICCV*, 2019. 2
- [13] N. Carlini and D. Wagner. Towards evaluating the robustness of neural networks. In *IEEE Symposium on Security and Privacy*, 2017. 1
- [14] P. Chen, Y. Sharma, H. Zhang, J. Yi, and C. Hsieh. Ead: Elastic-net attacks to deep neural networks via adversarial examples. In *AAAI*, 2018. 1
- [15] S. Cheng, Y. Dong, T. Pang, H. Su, and J. Zhu. Improving black-box adversarial attacks with a transfer-based prior. In *NeurIPS*, 2019. 2
- [16] F. Croce, M. Andriushchenko, and M. Hein. Provable robustness of relu networks via maximization of linear regions. In *AISTATS*, 2019. 3
- [17] F. Croce and M. Hein. Sparse and imperceivable adversarial attacks. In *ICCV*, 2019. 1, 2, 4, 5, 6, 12, 13, 14, 15
- [18] F. Croce and M. Hein. Minimally distorted adversarial examples with a fast adaptive boundary attack. In *ICML*, 2020. 1
- [19] Y. Dong, F. Liao, T. Pang, H. Su, J. Zhu, X. Hu, and J. Li. Boosting adversarial attacks with momentum. In *CVPR*, 2018. 8, 9, 17, 18

- [20] Y. Fan, B. Wu, T. Li, Y. Zhang, M. Li, Z. Li, and Y. Yang. Sparse adversarial attack via perturbation factorization. In *ECCV*, 2020. 5, 12, 13
- [21] A. Fawzi and P. Frossard. Measuring the effect of nuisance variables on classifiers. In *British Machine Vision Conference (BMVC)*, 2016. 2, 16
- [22] P. Flajolet, D. Gardy, and L. Thimonier. Birthday paradox, coupon collectors, caching algorithms and self-organizing search. *Discrete Applied Mathematics*, 39(3):207–229, 1992. 4
- [23] K. Grosse, N. Papernot, P. Manoharan, M. Backes, and P. McDaniel. Adversarial perturbations against deep neural networks for malware classification. *arXiv preprint arXiv:1606.04435*, 2016. 2, 6, 14
- [24] C. Guo, J. R. Gardner, Y. You, A. G. Wilson, and K. Q. Weinberger. Simple black-box adversarial attacks. In *ICML*, 2019. 2
- [25] J. E. Hu, A. Swaminathan, H. Salman, and G. Yang. Improved image Wasserstein attacks and defenses. *arXiv preprint arXiv:2004.12478*, 2020. 1
- [26] W. Hu and Y. Tan. Generating adversarial malware examples for black-box attacks based on GAN. *arXiv preprint arXiv:1702.05983*, 2017. 6
- [27] Z. Huang and T. Zhang. Black-box adversarial attack with transferable model-based embedding. In *ICLR*, 2020. 2
- [28] A. Ilyas, L. Engstrom, A. Athalye, and J. Lin. Black-box adversarial attacks with limited queries and information. *ICML*, 2018. 2, 4, 13
- [29] A. Ilyas, L. Engstrom, and A. Madry. Prior convictions: Black-box adversarial attacks with bandits and priors. *ICLR*, 2019. 2, 13
- [30] D. Jin, Z. Jin, J. T. Zhou, and P. Szolovits. Is BERT really robust? natural language attack on text classification and entailment. In *AAAI*, 2019. 2
- [31] D. Karmon, D. Zoran, and Y. Goldberg. Lavan: Localized and visible adversarial noise. In *ICML*, 2018. 1, 6, 8
- [32] A. Kurakin, I. J. Goodfellow, and S. Bengio. Adversarial examples in the physical world. In *ICLR Workshop*, 2017. 1, 6
- [33] C. Laidlaw, S. Singla, and S. Feizi. Perceptual adversarial robustness: Defense against unseen threat models. *arXiv preprint arXiv:2006.12655*, 2020. 1
- [34] M. Lee and Z. Kolter. On physical adversarial patches for object detection. *ICML Workshop on Security and Privacy of Machine Learning*, 2019. 1
- [35] J. Li, F. Schmidt, and Z. Kolter. Adversarial camera stickers: A physical camera-based attack on deep learning systems. In *ICML*, pages 3896–3904, 2019. 1
- [36] X. Liu, X. Du, X. Zhang, Q. Zhu, H. Wang, and M. Guizani. Adversarial samples on android malware detection systems for IoT systems. *Sensors*, 19(4):974, 2019. 2, 6
- [37] A. Madry, A. Makelov, L. Schmidt, D. Tsipras, and A. Valdu. Towards deep learning models resistant to adversarial attacks. In *ICLR*, 2018. 1, 5, 6, 8, 9, 17, 18
- [38] L. Meunier, J. Atif, and O. Teytaud. Yet another but more efficient black-box adversarial attack: tiling and evolution strategies. *arXiv preprint, arXiv:1910.02244*, 2019. 2
- [39] A. Modas, S. Moosavi-Dezfooli, and P. Frossard. Sparsefool: a few pixels make a big difference. In *CVPR*, 2019. 1, 5, 13
- [40] S.-M. Moosavi-Dezfooli, A. Fawzi, and P. Frossard. Deepfool: a simple and accurate method to fool deep neural networks. In *CVPR*, pages 2574–2582, 2016. 1
- [41] N. Narodytska and S. Kasiviswanathan. Simple black-box adversarial attacks on deep neural networks. In *CVPR Workshops*, 2017. 1, 2, 4
- [42] N. Papernot, P. McDaniel, S. Jha, M. Fredrikson, Z. B. Celik, and A. Swami. The limitations of deep learning in adversarial settings. In *2016 IEEE European symposium on security and privacy (EuroS&P)*, pages 372–387. IEEE, 2016. 1, 4, 5, 6, 12, 13, 14
- [43] R. Podschwadt and H. Takabi. On effectiveness of adversarial examples and defenses for malware classification. In *International Conference on Security and Privacy in Communication Systems*, pages 380–393. Springer, 2019. 6
- [44] A.-A. Pooladian, C. Finlay, T. Hoheisel, and A. M. Oberman. A principled approach for generating adversarial images under non-smooth dissimilarity metrics. In *AISTATS*, 2020. 1, 5
- [45] S. Rao, D. Stutz, and B. Schiele. Adversarial training against location-optimized adversarial patches. In *ECCV Workshop on the Dark and Bright Sides of Computer Vision: Challenges and Opportunities for Privacy and Security*, 2020. 6, 7, 15

- [46] L. Rastrigin. The convergence of the random search method in the extremal control of a many parameter system. *Automaton & Remote Control*, 24:1337–1342, 1963. 2
- [47] J. Rauber, W. Brendel, and M. Bethge. Foolbox: A python toolbox to benchmark the robustness of machine learning models. In *ICML Reliable Machine Learning in the Wild Workshop*, 2017. 13
- [48] J. Rony, L. G. Hafemann, L. S. Oliveira, I. B. Ayed, R. Sabourin, and E. Granger. Decoupling direction and norm for efficient gradient-based l2 adversarial attacks and defenses. In *CVPR*, pages 4322–4330, 2019. 1
- [49] L. Schott, J. Rauber, M. Bethge, and W. Brendel. Towards the first adversarially robust neural network model on MNIST. In *ICLR*, 2019. 1, 2, 4, 5
- [50] M. Seungyong, A. Gaon, and O. S. Hyun. Parsimonious black-box adversarial attacks via efficient combinatorial optimization. In *ICML*, 2019. 2
- [51] J. W. Stokes, D. Wang, M. Marinescu, M. Marino, and B. Bussone. Attack and defense of dynamic analysis-based, adversarial neural malware classification models. *arXiv preprint arXiv:1712.05919*, 2017. 6
- [52] C. Szegedy, W. Zaremba, I. Sutskever, J. Bruna, D. Erhan, I. Goodfellow, and R. Fergus. Intriguing properties of neural networks. In *ICLR*, pages 2503–2511, 2014. 1, 6
- [53] S. Thys, W. Van Ranst, and T. Goedemé. Fooling automated surveillance cameras: adversarial patches to attack person detection. In *CVPR Workshops*, 2019. 1
- [54] C.-C. Tu, P. Ting, P.-Y. Chen, S. Liu, H. Zhang, J. Yi, C.-J. Hsieh, and S.-M. Cheng. Autozoom: Autoencoder-based zeroth order optimization method for attacking black-box neural networks. In *AAAI*, 2019. 2
- [55] J. Uesato, B. O’Donoghue, A. Van den Oord, and P. Kohli. Adversarial risk and the dangers of evaluating against weak attacks. In *ICML*, 2018. 2
- [56] E. Wong, F. R. Schmidt, and J. Z. Kolter. Wasserstein adversarial examples via projected sinkhorn iterations. In *ICML*, 2019. 1
- [57] C. Yang, A. Kortylewski, C. Xie, Y. Cao, and A. Yuille. Patchattack: A black-box texture-based attack with reinforcement learning. In *ECCV*, 2020. 2, 6, 7, 9, 16
- [58] Z. B. Zabinsky. Random search algorithms. *Wiley encyclopedia of operations research and management science*, 2010. 3
- [59] M. Zajac, K. Zołna, N. Rostamzadeh, and P. O. Pinheiro. Adversarial framing for image and video classification. In *AAAI*, pages 10077–10078, 2019. 1, 7, 8, 16
- [60] R. Zhang, P. Isola, A. A. Efros, E. Shechtman, and O. Wang. The unreasonable effectiveness of deep features as a perceptual metric. In *CVPR*, pages 586–595, 2018. 1
- [61] P. Zhao, S. Liu, P.-Y. Chen, N. Hoang, K. Xu, B. Kailkhura, and X. Lin. On the design of black-box adversarial examples by leveraging gradient-free optimization and operator splitting method. In *ICCV*, pages 121–130, 2019. 2, 4, 5, 12, 13, 14

Appendix

Organization of the appendix

The appendix contains several additional results that we omitted from the main part of the paper due to the space constraints, as well as additional implementation details for each method. The organization of the appendix is as follows:

- Sec. **A**: additional results and implementation details of l_0 -bounded attacks on ImageNet where we also present results of *targeted* attacks.
- Sec. **B**: implementation details for l_0 -bounded attacks on malware detection.
- Sec. **C**: implementation details for generating image- and location-specific adversarial patches.
- Sec. **D**: implementation details for generating image-specific frames.
- Sec. **E**: results of universal attacks, i.e. image- and location-independent attacks, which include targeted universal patches and targeted universal frames.
- Sec. **F**: theoretical analysis of the l_0 -RS algorithm.
- Sec. **G**: ablation studies for l_0 -RS and Patch-RS.

A. l_0 -bounded attacks: image classification

In this section, we first describe the results of targeted attacks, then we show additional statistics for untargeted attacks, and describe the hyperparameters used for l_0 -RS and competing methods.

A.1. Targeted attacks

Here we test l_0 -bounded attacks in the targeted scenario using the sparsity level $k = 150$ (maximum number of perturbed pixels). We compare our l_0 -RS to PGD₀ [17], which is the strongest white-box attack from the prior work, and several other methods that provide implementations of targeted attacks. We additionally adapt CornerSearch [17], which is the strongest black-box attack (albeit not query efficient due to the initial phase that requires 400k queries), to the targeted setting. We set the query budget to 100,000, and show the success rate on VGG and ResNet in Table 6 computed on 500 points. The target class for each point is randomly sampled from the set of labels which excludes the true label. We report the success rate in Table 6 instead of robust error since we are considering targeted attacks where the overall goal is to cause a misclassification towards a particular class instead of an arbitrary misclassification. We can see that targeted attacks are more challenging than untargeted attacks for many methods, particularly for methods

attack	type	$k = 150$ (pixels)	
		VGG	ResNet
SAPF* [20]	white-box	0.0%	0.0%
JSMA-CE [42]	white-box	0.4%	1.4%
PGD ₀ [17]	white-box	62.8%	67.8%
JSMA-CE [42] w/ GE	black-box	0.0%	0.0%
PGD ₀ [17] w/ GE	black-box	0.4%	1.4%
CornerSearch* [17]	black-box	3.0%	2.0%
l_0 -RS	black-box	98.2%	95.6%

Table 6. Success rate of targeted l_0 -attacks with sparsity $k = 150$ pixels on ImageNet. The entries with * are evaluated on 100 points instead of 500 because of their high computational cost. All black-box attacks use 100k queries except CornerSearch which uses 450k. l_0 -RS outperforms all black- and white-box attacks.

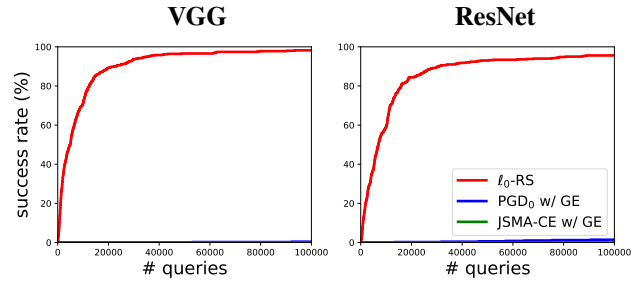


Figure 7. Success rate over queries for targeted black-box attacks in the l_0 -threat model with $k = 150$.



Figure 8. Targeted l_0 adversarial examples generated by our l_0 -RS algorithm for $k = 150$ pixels.

like CornerSearch that were designed primarily for untargeted attacks.

We report the query efficiency curves in Fig. 7 for l_0 -RS, PGD₀ and JSMA-CE with gradient estimation. We omit the ADMM attack [61] since it has shown the lowest success rate in the untargeted setting. We can see that l_0 -RS achieves a high success rate (90%/80% for VGG/ResNet) even after 20,000 queries. At the same time, the targeted setting is very challenging for other methods that have nearly 0% success rate even after 100,000 queries.

Finally, we visualize targeted l_0 adversarial examples generated by l_0 -RS in Fig. 8.

A.2. Additional statistics for targeted and untargeted attacks

In Table 7, we report the details of success rate and query efficiency of the black-box attacks on ImageNet for sparsity levels $k \in \{50, 150\}$ and 10,000/100,000 query limit for untargeted/targeted attacks respectively.

A.3. l_0 -RS algorithm

As mentioned in Sec. 4, at iteration i the new set M' is formed modifying $\alpha^{(i)} \cdot k$ (rounded to the closest positive integer) elements of M containing the currently modified dimensions (see step 6 in Alg. 1). Inspired by the step-size reduction in gradient-based optimization methods, we progressively reduce $\alpha^{(i)}$. Assuming $N = 10,000$, the schedule of $\alpha^{(i)}$ is piecewise constant where the constant segments start at iterations $j \in \{0, 50, 200, 500, 1000, 2000, 4000, 6000, 8000\}$ with values $\alpha_{\text{init}}/\beta_j$, $\beta_j \in \{2, 4, 5, 6, 8, 10, 12, 15, 20\}$. For a different maximum number of queries N , the schedule is linearly rescaled accordingly. In practice, we use $\alpha_{\text{init}} = 0.3$ and $\alpha_{\text{init}} = 0.1$ for the untargeted and targeted scenario respectively.

A.4. Competitors

SparseFool. We use SparseFool [39] as implemented in Foolbox [47] and optimize the hyperparameter which controls the sparsity of the solutions (called λ , setting finally $\lambda = 1$) to achieve the best results. The implementation in Foolbox has other two hyperparameters: we use 60 steps and 10 subsamples (default values are 30 and 10), after checking that higher values do not lead to improved performance but significantly increase the computational cost.

PGD₀. For PGD₀ [17] we use 2,000 iterations (5,000 for targeted attacks) and step size $0.05 \cdot d$ ($0.025 \cdot d$ for targeted attacks) where $d = 224 \times 224 \times 3$ is the input dimension. PGD₀ with gradient estimation uses the same gradient step of PGD₀ but with step size $5 \cdot d$ ($1 \cdot d$ for targeted attacks). To estimate the gradient we use finite differences, similarly to [28], as shown in Alg. 2, with the current iterate as input x , $\eta = 0.01/\sqrt{d}$ (in line with what suggested in [29] for this algorithm), $m = 1$ and a zero vector as p . In case of targeted attacks we instead use $m = 50$ (the budget of queries is also 10 times larger) and the current estimated gradient as p . We optimized the aforementioned parameters to achieve the best results and tested that sampling more points to better approximate the gradient at each iteration leads to similar success rate with worse query consumption.

CornerSearch. For CornerSearch, we used the following hyperparameters: $n_{\text{max}} = 500$, $n_{\text{iter}} = 200$, $n_{\text{classes}} = 1,000$ (i.e. all classes, which is the default option) for untargeted attacks and $n_{\text{max}} = 1,500$, $n_{\text{iter}} = 50,000$ for targeted attacks. We note that CornerSearch has a limited scalability to ImageNet as it re-

Algorithm 2: GradEst: Gradient estimation via finite differences

input : loss function L , input point x , number of iterations m , step size η , prior estimation p
output: estimated gradient g

```

1  $g \leftarrow p$ 
2 for  $i = 1, \dots, m$  do
3    $s \leftarrow \mathcal{N}(0, I)$ 
4    $l_1 \leftarrow L(x + \eta \cdot s)$ 
5    $l_2 \leftarrow L(x - \eta \cdot s)$ 
6    $g \leftarrow g + (l_1 - l_2)/(2\eta) \cdot s$ 
```

quires $8 \cdot 224 \cdot 224 = 401,408$ queries only for the initial phase of the attack to obtain the orderings of pixels, and then for the second phase $n_{\text{iter}} \cdot n_{\text{classes}} = 200,000$ queries for untargeted attacks and $n_{\text{iter}} = 50,000$ queries for targeted attacks. Thus, CornerSearch requires significantly more queries compared to l_0 -RS while achieving a lower success rate. Finally, we note that CornerSearch was designed to minimize the number of modified pixels, while we use it here for l_0 -bounded attacks.

SAPF. For SAPF [20], we use the hyperparameters suggested in their paper and we use the second-largest logit as the target class for untargeted attacks. With these settings, the algorithm is still very expensive computationally, so we could evaluate it only on 100 points. Note that [20] report that SAPF achieves the average l_0 -norm of at least 30,000 which is orders of magnitudes more than what we consider here. But we evaluate it for completeness as their goal is to obtain a sparse adversarial attack measured in terms of l_0 .

ADMM. For ADMM [61] we perform a grid search over the parameters to optimize the success rate and set $\text{ro}=10$, $\text{gama}=4$, $\text{binary_search_steps}=500$ and $\text{Query_iterations}=20$ (other parameters are used with the default values). Note that [61] report results for the l_0 -norm only on MNIST.

JSMA-CE. As mentioned in Sec. 4.2 we adapt the method introduce in [42] to scale it to attack models on ImageNet. We build the saliency map as the gradient of the cross-entropy loss instead of using the gradient of the logits because ImageNet has 1000 classes and it would be very expensive to get gradients of each logit separately (particularly in the black-box settings where one has to first estimate them). Moreover, at each iteration we perturb the pixel which has the gradient with the largest l_1 -norm, setting each channel to either 0 or 1 according to the sign of the gradient at it. We perform these iterations until the total sparsity budget is reached. For the black-box version, we modify the algorithm as follows: the gradient is estimated via finite difference approximation as in Alg. 2, the original image x_{orig} as input throughout the whole procedure (this means that the prior p is always the current estimation of the gra-

		attack	VGG			ResNet		
			succ. rate	mean queries	med. queries	succ. rate	mean queries	med. queries
untargeted	$k = 50$	ADMM [61]	8.3%	9402	10000	8.8%	9232	10000
		JSMA-CE [42] w/ GE	33.5%	7157	10000	29.0%	7509	10000
		PGD ₀ [17] w/ GE	49.1%	5563	10000	38.0%	6458	10000
		l_0 -RS	97.6%	737	88	94.6%	1176	150
	$k = 150$	ADMM [61]	16.9%	8480	10000	14.2%	8699	10000
		JSMA-CE [42] w/ GE	58.8%	4692	2460	49.4%	5617	10000
		PGD ₀ [17] w/ GE	68.1%	3447	42	59.4%	4263	240
		l_0 -RS	100%	171	25	100%	359	49
targeted	$k = 150$	JSMA-CE [42] w/ GE	0.0%	100000	100000	0.0%	100000	100000
		PGD ₀ [17] w/ GE	0.4%	99890	100000	1.4%	99357	100000
		l_0 -RS	98.2%	9895	4914	95.6%	14470	6960

Table 7. We report the success rate and statistics about query consumption of black-box l_0 -bounded attacks on ImageNet. We consider sparsity levels $k \in \{50, 150\}$ and compute the average and median number of queries needed to generate adversarial examples on all correctly classified points.

dient). We found that this gives stronger results compared to an estimation of the gradient at a new iterate. We use the gradient estimation step size $\eta = 0.01$. Then every 10 queries we perturb the k pixels with the largest gradient as described above for the white-box attack and check whether this new image is misclassified (we do not count this extra query for the budget of 10k). This is in line with the version of the attack we use for the malware detection task in Sec. 4.4 and described in detail in Sec. B.

B. l_0 -bounded attacks: malware detection

Dataset. The Drebin dataset [6] consists of 129,013 Android applications, among which 123,453 are benign and 5,560 malicious, with $d = 545,333$ features divided into 8 families. Data points are represented by a binary vector $x \in \{0, 1\}^d$ indicating whether each feature is present or not in x .

Experimental setup. As [23], we restrict the attacks to only adding features from the first 4 families, that is modifications to the manifest of the applications, to preserve the functionality of the samples (no feature present in the clean data is removed), which leaves a maximum of 233,727 alterable dimensions. Only adding features means that all values in Δ equal 1, thus $\Delta' \equiv \Delta$ at every iteration (step 7 in Alg. 1) and only the set M is updated. For our attack we use $\alpha_{\text{init}} = 1.6$ and the same schedule of $\alpha^{(i)}$ of l_0 -RS on image classification tasks (see Sec. A).

Model. We trained the classifier, which has 1 fully-connected hidden layer with 200 units and uses ReLU as activation function, with 20 epochs of SGD minimizing the cross-entropy loss, with a learning rate of 0.1 reduced by a factor of 10 after 10 and 15 epochs. We use batches of size 2000, consisting of 50% of benign and 50% of malicious examples. For training, we merged the training and validation sets of one of the splits provided by [6]. It achieves a

Algorithm 3: JSMA-CE with gradient estimation (malware detection)

input : cross-entropy loss L , input point x_{orig} , number of iterations N , pixel budget k , number of iterations for gradient estimation m , gradient estimation step size η

output: z

```

1  $g \leftarrow \mathbf{0}, \quad q \leftarrow 2 \cdot m$ 
2 while  $q \leq N$  do
3    $g \leftarrow \text{GradEst}(L, x_{\text{orig}}, m, \eta, g)$ 
4    $z \leftarrow x_{\text{orig}}$ 
5    $A \leftarrow$  indices of  $k$  largest positive components of  $g$  (if there are)
6    $z_A \leftarrow 1$ 
7    $q \leftarrow q + 2 \cdot m$ 
8   if  $z$  is adversarial then return;
```

test accuracy of 98.85%, with a false positive rate of 1.01%, and a false negative rate of 4.29%.

B.1. Competitors

JSMA-CE with gradient estimation. The idea of the white-box attack of [23] is, given a sparsity level of k , to perturb iteratively the feature of the iterate $x^{(i)}$ which corresponds to the largest value (if positive) of $\nabla_x L_{\text{CE}}(f(x^{(i)}), y)$, with f the classifier, y the correct label and L_{CE} the cross-entropy loss, until either the maximum number of modifications are made or misclassification is achieved. With only approximate gradients this approach is not particularly effective. However, since $k \ll d$ and only additions can be made, we aim at estimating the gradient of the cross-entropy loss at x_{orig} and then set to 1 the k elements (originally 0) of x_{orig} with the largest component

in the approximated gradient. With the goal of query efficiency, every m iterations of gradient estimation through finite differences we check if an adversarial example has been found (we do not count these queries in the total for the query limit). Alg. 3 shows the procedure, and for the main experiments in Sec. 4.4 we set $m = 5$ and $\eta = 1$ (we tested other values which achieved worse or similar performance).

PGD₀ with gradient estimation. We use PGD₀ [17] with the gradient estimation technique presented in Alg. 2 with the original point as input x , $m = 10$, $\eta = 100$ and the current estimate of the gradient as prior p (unlike on image classification tasks where the gradient is estimated at the current iterate and no prior used). Moreover, we use step size $4 \cdot \sqrt{d}$ and modify the projection step the binary input case and so that features are only added and not removed (see above).

C. Image- and location-specific adversarial patches

We here report the details of the attacks for image- and location-specific adversarial patches.

C.1. Patch-RS algorithm

As mentioned in Sec. 5, in this scenario we optimize via random search the attacks for each image independently. In Patch-RS we alternate iterations where a candidate update of the patch is sampled with others where a new location is sampled.

Location updates. We have a location update every m iterations, with $m = 5$ (1 : 4 scheme Sec. G.2, four patch updates then one location update) for untargeted attacks and $m = 10$ for targeted ones: the latter have more queries available (50k vs 10k) and wider patches (40×40 vs 20×20), therefore it is natural to dedicate a larger fraction of iterations to optimizing the content rather than the position (which has also a smaller feasible set). We present in Sec. G.2 an ablation study the effect of different frequencies of location updates in the untargeted scenario. The position of the patch is updated with an uniformly sampled shift in $[-h^{(i)}, h^{(i)}]$ for each direction (plus clipping to the image size if necessary), where $h^{(i)}$ is linearly decreased from $h^{(0)} = 0.75 \cdot s_{\text{image}}$ to $h^{(N)} = 0$ (s_{image} indicates the side of the squared images). In this way, initially, the patch can be easily moved on the image, while towards the final iterations it is kept (almost) fixed and only its values are optimized.

Patch updates. The patch is initialized by superposing at random positions on a black image 1000 squares of random size and color in $\{0, 1\}^3$. Then, we update the patch following the scheme of Square Attack [4], that is sampling random squares with color one of the corners of the

color cube and accept the candidate if it improves the target loss. The size of the squares is decided by a piecewise constant schedule, which we inherit from [4]. Specifically, at iteration i the square-shaped updates of a patch with size $s \times s$ have side length $s^{(i)} = \sqrt{\alpha^{(i)}} \cdot s$, where the value of $\alpha^{(i)}$ starts with $\alpha^{(0)} = \alpha_{\text{init}}$ and then is halved at iteration $j \in \{10, 50, 200, 500, 1000, 4000, 8000\}$ if the query limit is $N = 10,000$, otherwise the values of j are linearly rescaled according to the new N . Hence, α_{init} is the only tunable parameters of Patch-RS, and we set $\alpha_{\text{init}} = 0.4$ for untargeted attacks and $\alpha_{\text{init}} = 0.1$ for targeted ones.

In contrast to Square Attack, in the second half of the iterations dedicated to updates of size 1×1 , Patch-RS performs a refinement of the patch applying only single-channel updates. We show in Sec. G.2 that both the initialization tailored for the specific threat model and the single-channel updates allow our algorithm to achieve the best success rate and query efficiency.

C.2. Competitors

Sparse-RS + SH and Sparse-RS + SA. When integrating SignHunter [2] and Square Attack [4] in our framework for adversarial patches, the updates of the locations are performed as described above, while the patches are modified with the l_∞ attacks with constraints given by the input domain $[0, 1]^d$ (in practice one can fix a sufficiently large l_∞ threshold $\epsilon_\infty = 1$). SH does not have free parameters, while we tune the only parameter p of SA (which has the same role as α_{init} of Patch-RS) and use $p = 0.4$ and $p = 0.2$ for the untargeted and targeted case respectively.

LOAP. Location-Optimized Adversarial Patches (LOAP) [45] is a white-box PGD-based attack which iteratively first updates the patch with a step in the direction of the sign of the gradient to maximize the cross-entropy function at the current iterate, then it tests if shifting of `stride` pixels the patch in one of the four possible directions improves the loss and, if so, the location is updated otherwise kept ([45] have also a version where only one random shift is tested). We use LOAP as implemented in <https://github.com/sukrutrao/Adversarial-Patch-Training> with 1,000 iterations, learning rate 0.05 and the full optimization of the location with `stride=5`. To adapt LOAP to the black-box setup, we use the gradient estimation via finite differences shown in Alg. 2 restricted to the patch to optimize (this means that the noise sampled in step 3 is applied only on the components of the image where the patch is). In particular we use the current iterate as input x , $m = 5$ iterations, $\eta = 10/(s \cdot \sqrt{c})$ if the patch has dimension $s \times s \times c$ and the gradient estimation at the previous iteration as prior p . Moreover, we perform the update of the location by sampling only 1 out of the 4 possible directions (as more queries are necessary for better gradient estimation) with

stride=5, and learning rate 0.02 for the gradient steps (the sign of the gradient is used as a direction). Note that we optimized these hyperparameters to achieve the best final success rate. Moreover, each iteration costs 11 queries (10 for Alg. 2 and 1 for location updates) and we iterate the procedure until the budget of queries is exhausted.

TPA. The second method we compare to is TPA [57], which is based on reinforcement learning and exploits a dictionary of patches. Note that in [57] TPA was used primarily putting multiple patches on the same image to achieve misclassification, while our threat model does not include this option. We obtained the optimal values for the hyperparameters for untargeted attacks (rl_batch=400 and steps=25) via personal communication with the authors and set those for the targeted scenario (rl_batch=1000 and steps=50) similarly to what reported in the original code at <https://github.com/Chenglin-Yang/PatchAttack>, doubling the value of rl_batch to match the budget of queries we allow. TPA has a mechanism of early stopping, which means that it might happen that not the whole budget of queries is exploited even for unsuccessful points. Finally, [57] show that TPA significantly outperforms the methods of [21], which also generates image-specific patches, although optimizing the shape and the location but not the values of the perturbation. Thus we do not compare directly to [21] in our experiments.

D. Image-specific adversarial frames

We here report the details of the attacks for image-specific adversarial frames.

D.1. Frames-RS algorithm

We initialize the components of the frame with random values in $\{0, 1\}$. Then, at each iteration i we sample uniformly a pixel of the frame to be a random corner of a square of size $s^{(i)} \times s^{(i)}$: all the pixels in the intersection of such square with the frame are set to the same randomly chosen color in $\{0, 1\}^c$ to create the candidate update. The length of the side of the square is regulated by a linearly decreasing schedule ($s^{(i)} = 3\lceil\alpha_{\text{init}} \cdot w^2 \cdot (0.5 - i/N)\rceil$, with N the total number of queries available and w the width of the frame) for the first 50% of queries, after which $s^{(i)} = 1$. Finally, for the last 75% of iterations, only single-channel updates are performed. Similarly to the other threat models, the only hyperparameter is α_{init} .

D.2. Competitors

Sparse-RS + SH and Sparse-RS + SA. SignHunter [2] can be directly used to generate adversarial frames as this method does not require a particular shape of the perturbation set. Square Attack is specifically designed for rectangular images and we adapted it to this setting by constraining the sampled updates to lay inside the frame, as they are

contained in the image for the l_∞ - and l_2 - threat models. Since the perturbation set has a different shape than in the other threat models a new schedule for the size of squares specific for this case: at iteration i of N and with frames of width w , we have $s^{(i)} = \lceil\alpha_{\text{init}} \cdot w \cdot (0.5 - i/N)\rceil$ until $i < N/2$, then $s^{(i)} = 1$ (we set $\alpha_{\text{init}} = 2$).

Adversarial framing (AF). In [59] propose a method based on gradient descent to craft universal adversarial frames. We here use standard PGD on the cross-entropy loss to generate image-specific perturbations by updating only the components corresponding to the pixels belonging to the frame. In details, we use 1000 iterations with step size 0.05 using the sign of the gradient as direction and each element is projected on the interval $[0, 1]$. This white-box attack achieves 100% of success in all settings we tested (consider that 1176 and 2652 pixels be perturbed for the untargeted and targeted scenarios respectively). For the black-box version, we use the gradient estimation technique as for patches (Sec. C), that is Alg. 2 with the current iterate as input x , $m = 5$, $\eta = 10/\sqrt{d}$ and the gradient estimated at the previous iteration as prior p , where d represents the number of features in the frame. Moreover, we use step size 0.1 for the untargeted case, 0.01 for the targeted one. Note that we found the mentioned values via grid search to optimize the success rate. We iterate the procedure, which costs 10 queries of the classifier, until reaching the maximum number of allowed queries or finding a successful adversarial perturbation.

E. Targeted universal attacks: patches and frames

We here report the additional results and implementation details of the attacks for targeted universal patches and frames.

E.1. Sparse-RS for targeted universal attacks

Targeted universal attacks have to generalize to unseen images and, in the case of patches, random locations on the image. We propose to generate them in a black-box scenario with the following scheme, with a budget of 100k iterations. We select a small batch of training images $\{x_i\}_{i=1}^n$ ($n = 30$) and apply the patch at random positions on them (for frames the location is determined by its width). This positions are kept fixed for 10k iterations during which the patch is updated (step 7 of Alg. 1) with some black-box attack (we use the same as for image-specific attacks in Sec. 5 and Sec. 6) to minimize the loss

$$L_{\text{targ}}(\{x_i\}_{i=1}^n) = \sum_{i=1}^n L_{\text{CE}}(f(x_i), t), \quad (3)$$

where t is the target class. Then, to foster generalization, we resample both the batch of training images and the lo-

cations of the patch over them (step 6 in Alg. 1). In this way it is possible to obtain black-box attacks without relying on surrogate models. Note that 30 queries of the classifiers are performed at every iteration of the algorithm.

In this scheme, as mentioned, we integrate either Sign-Hunter [2] or Square Attack [4] to have Sparse-RS + SH and Sparse-RS + SA, and our novel Patch-RS introduced for image-specific attacks. In the case of patches, for Sparse-RS + SA we set $p = 0.05$ and for Patch-RS $\alpha_{\text{init}} = 0.05$ (recall that both parameters control the schedule for sampling the updates in a similar way for the two attacks, details in Sec. C). For frames, for SA we use the schedule for image-specific attacks (Sec. D) with $\alpha_{\text{init}} = 0.7$, while in Frame-RS we adapt the schedule for image-specific attacks to the specific case, so that the size of the squares decrease to $s^{(i)} = 1$ at $i = 25,000$ and single-channel updates are sampled from $i = 62,500$.

E.2. Transfer-based attacks

We evaluate the performance of targeted universal patches and frames generated by PGD [37] and MI-FGSM [19] on a surrogate model and then transferred to attack the target model. In particular, at every iteration of the attack we apply on the training images (200) the patch at random positions (independently picked for every image), average the gradients of the cross-entropy loss at the patch for all images, and take a step in the direction of the sign of the gradients (we use 1000 iterations, step size of 0.05 and momentum coefficient 1 for MI-FGSM). For patches, we report the success rate as the average over 500 images, 10 random target classes, and 100 random positions of the patches for each image. For frames, we average over 5000 images and the same 10 random target classes. In Table 8 we show the success rate of the transfer based attacks on the surrogate model but with images unseen when generating the perturbation and on the target model (we use VGG and ResNet alternatively as the source and target models). We see that the attacks achieve a very high success rate when applied to new images on the source model, but are not able to generalize to another architecture. We note that [11] also report a similarly low success rate for the same size of the patch (50×50 which corresponds to approximately 5% of the input image, see Fig. 3 in [11]) on the target class they consider. Finally, we note that [19] show that the perturbations obtained with MI-FGSM have better transferability compared to PGD, while in our experiments they are slightly worse, but we highlight that such observation was done for image-specific l_∞ - and l_2 -attacks, which are significantly different threat models from what we consider here.

		succ. rate			
		V \rightarrow V	V \rightarrow R	R \rightarrow R	R \rightarrow V
patches	PGD [37]	99.6%	0.0%	94.9%	3.3%
	MI-FGSM [19]	99.1%	0.0%	92.6%	1.3%
frames	PGD [37]	99.4%	0.0%	99.8%	0.0%
	MI-FGSM [19]	99.3%	0.0%	99.7%	0.0%

Table 8. Success rate of transfer-based targeted universal patches, with VGG (V) and ResNet (R) used as either source or target model averaged over 10 classes. When source and target model are the same network, the attack is only used on unseen images. These targeted universal attacks are very effective when transferred to unseen images on the source model, but do not generalize to the other architecture.

E.3. Targeted universal attacks via gradient estimation

Consistently with the other threat models, we test a method based on PGD with gradient estimation. In particular, in the scheme introduced in Sec. E.1 for Sparse-RS, we optimize the loss with the PGD attack [37] and the gradient estimation technique via finite differences as in Alg. 2, similarly to what is done for image-specific perturbations in Sec. C and Sec. D (we also use the same hyperparameters, step size 0.1 for PGD).

E.4. Additional results

To evaluate the success of a targeted universal patch, we apply to each of 500 images the patch at 100 random locations and compute the percentage of the perturbed images which are classified in the target class. For targeted universal frames, we compute the success rate applying the perturbation to 5,000 images (unseen during training). The results in Table 5 in Sec. 7 are computed as mentioned above for 10 randomly chosen target classes and then averaged (the same set of target classes is used for patches and frames). For the random search based attacks, we repeat the attacks for 3 random seeds. We report the complete results for both threat models in Table 9. Visualizations of the perturbations found by our scheme are shown in Fig. 9. Finally, we report the details of the success rate on each class in Table 10 for adversarial patches and Table 11 for adversarial frames.

F. Theoretical analysis of l_0 -RS

In this section we prove the following proposition which shows that l_0 -RS requires a sublinear number of queries (improving upon the linear number of queries needed by naive gradient estimation approaches).

Proposition 4.1 *The expected number t_k of queries needed for l_0 -RS with $\alpha^{(i)} = 1/k$ to find a set of k weights out of*

attack	patches		frames	
	VGG	ResNet	VGG	ResNet
Transfer PGD [37]	3.3%	0.0%	0.0%	0.0%
Transfer MI-FGSM [19]	1.3%	0.0%	0.0%	0.0%
PGD w/ GE	35.1%	15.5%	22.7%	52.4%
Sparse-RS + SH [2]	63.9%	13.8%	48.8%	65.5%
Sparse-RS + SA [4]	72.9% ± 3.6	29.6% ± 5.6	43.0% ± 1.2	63.6% ± 2.1
Patch-RS / Frame-RS	70.8% ± 1.3	30.4% ± 8.0	55.5% ± 0.3	65.3% ± 2.3

Table 9. Average success rate of targeted universal attacks over 10 target classes on VGG and ResNet. We use patches of size 50×50 and frames of width 6 pixels and repeat the attacks based on random search with 3 random seeds.

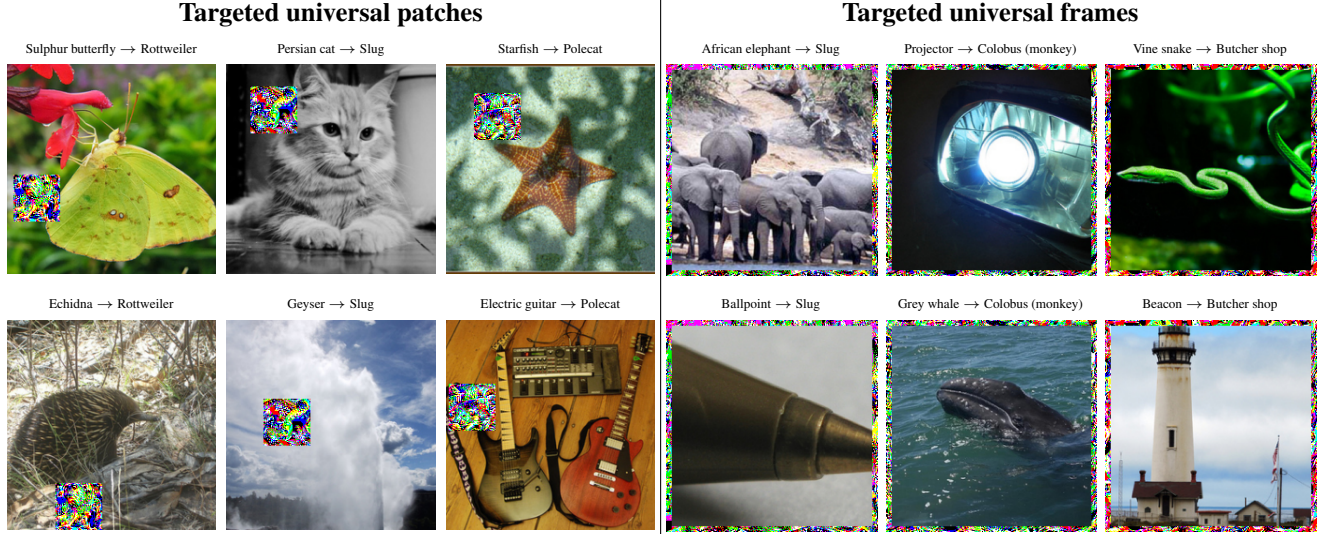


Figure 9. Targeted universal patches and frames generated by our Patch-RS and Frame-RS. We show two images in each column with the same universal patch/frame that is able to change the decision of the classifier into the desired target class.

the smallest m weights of a linear model is:

$$\mathbb{E}[t_k] = (d-k)k \sum_{i=0}^{k-1} \frac{1}{(k-i)(m-i)} < (d-k)k \frac{\ln(k) + 2}{m-k}.$$

Proof. According to the l_0 -RS algorithm, we have d features grouped in a set U and the goal is to find a set $M \subset U$ containing k elements among the m smallest elements of U . Since $\alpha^{(i)} = 1/k$, at every iteration we pick one element $p \in M$ to remove from M and one element $q \in U \setminus M$ to add to M . This results in a binary vector $z_{new} \in \{0, 1\}^d$ indicating which are the features in M . Then we query the black-box linear model to determine whether the loss at a new point z_{new} improves compared to the point on the previous iteration $z_{current}$, i.e. $L(z_{new}) < L(z_{current})$, which gives us information whether $q < p$.

If the current set M contains i elements which belong to the smallest m , the probability of increasing it to $i+1$ elements with the next pick is equal to

$$\begin{aligned} \mathcal{P}[i \rightarrow i+1] &= \mathcal{P}[p \notin \text{smallest } m, q \in \text{smallest } m] \\ &= \frac{k-i}{k} \cdot \frac{m-i}{d-k}. \end{aligned}$$

Then the expected number of iterations for the step $i \rightarrow i+1$ is equal to

$$\mathbb{E}[t_{i+1} - t_i] = \frac{(d-k)k}{(k-i)(m-i)}$$

since all the draws are independent. Assuming that we begin with none of the smallest m elements in M , the expected number of iterations t_k needed to find a set of k weights out of the smallest m weights is given by

$$\begin{aligned} \mathbb{E}[t_k] &= \sum_{i=0}^{k-1} \mathbb{E}[t_{i+1} - t_i] = \sum_{i=0}^{k-1} \frac{(d-k)k}{(k-i)(m-i)} \\ &= (d-k)k \sum_{i=0}^{k-1} \frac{1}{(k-i)(m-i)}. \end{aligned} \tag{4}$$

Now assuming that $m > k$, we can write the summation as:

$$\begin{aligned}
\sum_{i=0}^{k-1} \frac{1}{(k-i)(m-i)} &= \sum_{j=1}^k \frac{1}{j(j+m-k)} \\
&= \frac{1}{m-k} \sum_{j=1}^k \left(\frac{1}{j} - \frac{1}{j+m-k} \right) \\
&= \frac{1}{m-k} (H_k - H_m + H_{m-k}),
\end{aligned} \tag{5}$$

where H_k is the k -th harmonic number. Using the fact that $\ln(k) < H_k \leq \ln(k) + 1$, we have

$$H_k - H_m + H_{m-k} < \ln(k) - \ln(m) + \ln(m-k) + 2$$

and

$$\ln(k) - \ln(m) + \ln(m-k) + 2 < \ln(k) + 2.$$

If we combine this result with Eq. (4) and Eq. (5), we obtain the desired upper bound on $\mathbb{E}[t_k]$:

$$\mathbb{E}[t_k] < (d-k)k \frac{\ln(k) + 2}{m-k}.$$

□

Remark F.1 We further remark that for $m = k$ we get that

$$\mathbb{E}[t_k] = (d-k)k \sum_{j=1}^k \frac{1}{j^2} < \frac{\pi^2}{6} (d-k)k,$$

however we are interested in the setting when the gap $m-k$ is large enough so that $\mathbb{E}[t_k]$ becomes sublinear.

The main conclusion from Proposition 4.1 is that $\mathbb{E}[t_k]$ becomes sublinear for large enough gap $m-k$ which we further illustrate in Fig. 10 where we plot the expected number of queries needed by l_0 -RS for $d = 150,528$ and $k = 150$ which is equivalent to our ImageNet experiments with 50 pixels perturbed.

G. Ablation studies

We here present a series of ablation studies to better understand the robustness of our algorithms to different random seeds, how its performance changes depending on α_{init} , and to justify the algorithmic choice of the piecewise decaying schedule for $\alpha^{(i)}$. We focus the ablation study only on l_0 -RS and Patch-RS methods since for other threat models the setting is less challenging as there is no need to optimize the location of the perturbation.

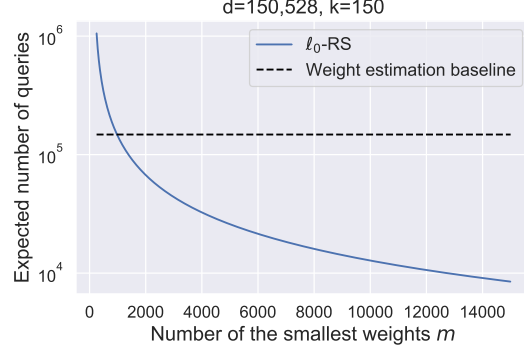


Figure 10. Comparison of the query efficiency of l_0 -RS to that of the naive weight estimation baseline which requires $O(d)$ queries to estimate the gradient.

G.1. l_0 -bounded attacks

Different random seeds. First, we study how the performance of l_0 -RS varies when using different random seeds, which influence the stochastic component inherent in random search. In Table 12 we report mean and standard deviation over 10 runs (with different seeds) of success rate, average and median queries of l_0 -RS on VGG and ResNet with sparsity levels $k \in \{50, 100, 150\}$ (the same setup of Sec. 4.2, with the additional $k = 100$). One can observe that the success rate is very stable in all the cases and the statistics of query consumption consistent across different runs.

Different values of α_{init} . Then we analyze the behaviour of our algorithm with different values of α_{init} , since it is the only free hyperparameter of Sparse-RS. Let us recall that it is used to regulate how much M' and Δ' differ from M and Δ respectively in steps 6-7 of Alg. 1 at each iteration. Fig. 11 shows the success rate and query usage (computed on the successful samples) of our untargeted l_0 -bounded attack on VGG at the usual three sparsity levels k for runs with $\alpha_{\text{init}} \in \{0.01, 0.05, 0.1, 0.2, 0.3, 0.4, 0.6, 0.8, 1\}$ (for our experiments in Sec. 4.2 we use $\alpha_{\text{init}} = 0.3$). We observe that the success rate is similar (close to 100%) for all the values, with a slight degradation for the largest ones. In order to minimize the queries of the classifier, the runs with α_{init} between 0.1 and 0.4 are comparably good, with small differences in the tradeoff between average and median number of queries.

Constant vs decaying $\alpha^{(i)}$. In order to demonstrate the role of decaying the difference between the candidate updates M' and Δ' and the current iterates M and Δ over iterations (see steps 6-7 of Alg. 1) to achieve good performance, we run our attack with constant $\alpha^{(i)}$ schedule instead of the piecewise constant schedule with decreasing values. We fix $\alpha^{(i)} = c \in [0, 1]$ for every i so that for the whole algorithm M' and M differ in $\max\{c \cdot k, 1\}$ elements. In Fig. 12 we report the results achieved by $c \in$

$\{0, 0.05, 0.15, 0.3, 0.5, 1\}$ on VGG at $k \in \{50, 100, 150\}$, together with the baseline (black dashed line) of the standard version of l_0 -RS. One can observe that small constant values c for $\alpha^{(i)} = c$ achieve a high success rate but suffer in query efficiency, in particular computed regarding the median and for larger k , while the highest values of c lead to significantly worse success rate (note that average and median queries are computed only on the successful points) than the baseline. These results highlight how important it is to have an initial exploration phase, with a larger step size, and at a later stage a more local optimization.

G.2. Image-specific adversarial patches

We here show the individual effect of our algorithmic choices to craft image-specific adversarial patches.

Initialization and single-channel updates. The original Square Attack [4] for l_∞ - and l_2 -bounded perturbations applies as initialization vertical stripes on the target image, and it does not consider updates of a single channel (these can be randomly sampled but are not explicitly performed). Table 13 shows the success rate and query efficiency (computed on all points) for untargeted adversarial attacks with patches of size 20×20 on VGG and ResNet, averaged over 5 random seeds for methods based on random search. Both the initialization with squares and the single-channel updates already individually improve the performance of Sparse-RS + SA and, when combined, allow Patch-RS to outperform the competitors (see also Sec. 5).

Ratio location to patch updates. We study here the effect of different ratios between the number of location and patch updates in our framework for image-specific untargeted patches (size 20×20). In Table 14 we report the performance Sparse-RS + SH, Sparse-RS + SA and our final method Patch-RS with various schemes: alternating an update of the location to one of the patch (1:1), doing 4 or 9 location updates for one patch update (4:1, 9:1) and vice versa (1:4, 1:9). Considering the results on both networks, the scheme with 1:4 ratio yields for every attack the highest success rate or very close. In query consumption, the schemes 1:1 and 1:4 are similar, with some trade-off between average and median. Moreover, we observe that the ranking of the three methods is preserved for all ratios of location and patch updates we tested, with Patch-RS outperforming the others. Also, its effectiveness is less affected by suboptimal ratios, showing the stability of our algorithm.

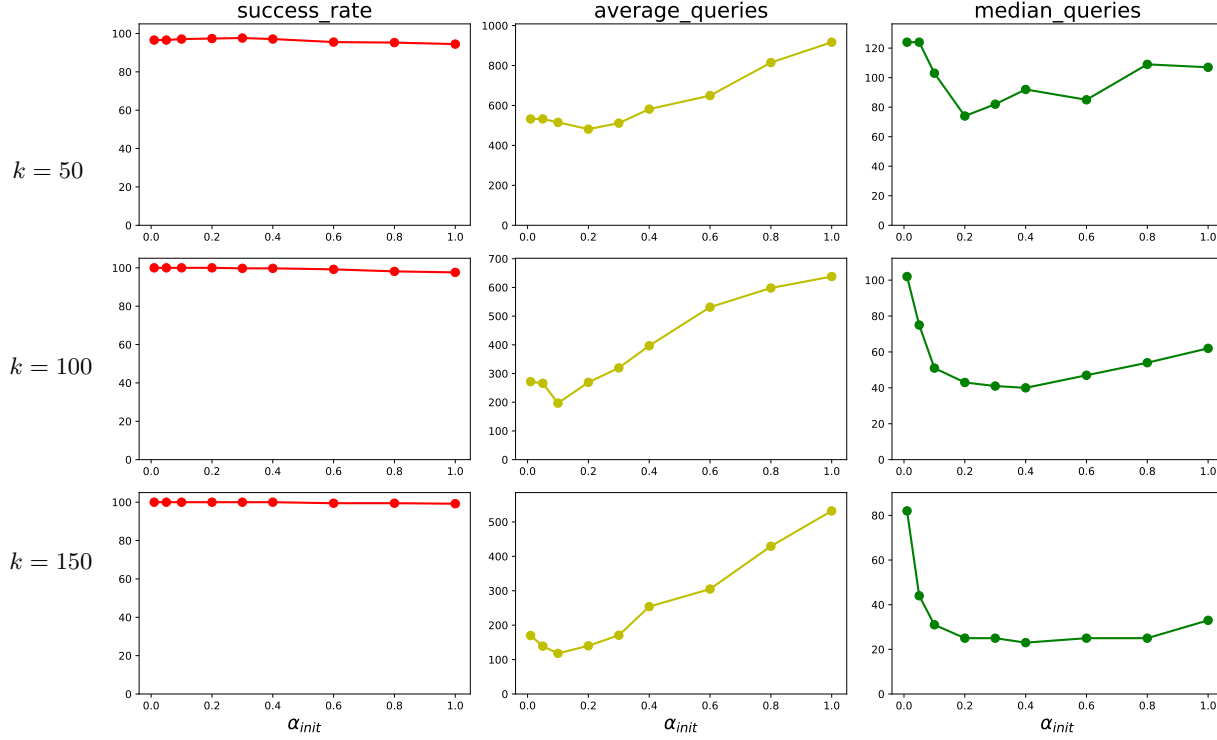


Figure 11. Ablation study on the influence of α_{init} , the hyperparameter which regulates the size of the updates at each iteration. We show success rate (first column), average (second) and median queries (third) achieved by l_0 -RS on VGG at sparsity levels $k = \{50, 100, 150\}$. Considering jointly the three statistics values in $[0.1, 0.4]$ are preferable for this threat model and schedule.

class	VGG			ResNet		
	Sparse-RS + SH	Sparse-RS + SA	Patch-RS	Sparse-RS + SH	Sparse-RS + SA	Patch-RS
Rottweiler	61.4%	77.1% \pm 14.6	83.4% \pm 3.9	0.2%	42.6% \pm 26.6	44.4% \pm 29.3
Lakeland terrier	65.4%	86.0% \pm 2.7	76.1% \pm 9.7	0.5%	0.6% \pm 0.2	12.2% \pm 14.8
polecat	46.7%	29.5% \pm 20.6	47.1% \pm 32.3	0.1%	27.3% \pm 15.5	15.0% \pm 9.7
waffle iron	86.3%	82.3% \pm 3.2	74.7% \pm 3.7	17.4%	16.2% \pm 3.9	18.6% \pm 4.9
whippet	37.7%	73.6% \pm 1.6	52.7% \pm 6.0	0.1%	36.9% \pm 24.0	35.4% \pm 24.0
digital clock	97.8%	97.6% \pm 0.2	97.0% \pm 0.5	90.5%	90.4% \pm 3.1	92.5% \pm 1.3
colobus	69.1%	68.9% \pm 5.2	80.1% \pm 4.7	0.0%	0.0% \pm 0.0	0.0% \pm 0.0
slug	61.0%	55.8% \pm 6.9	68.1% \pm 4.8	27.9%	43.7% \pm 1.7	44.2% \pm 10.7
butcher shop	42.4%	67.4% \pm 2.1	44.1% \pm 31.1	1.8%	2.4% \pm 0.6	1.0% \pm 0.5
bluetick	71.3%	90.5% \pm 1.1	85.0% \pm 2.4	0.0%	35.8% \pm 18.5	40.9% \pm 19.5

Table 10. Success rate of targeted universal patches for each of the 10 randomly chosen target classes.

class	VGG			ResNet		
	Sparse-RS + SH	Sparse-RS + SA	Frame-RS	Sparse-RS + SH	Sparse-RS + SA	Frame-RS
Rottweiler	39.4%	34.9% \pm 7.5	61.8% \pm 8.5	79.9%	77.6% \pm 4.5	81.6% \pm 8.2
Lakeland terrier	60.3%	45.6% \pm 9.7	69.9% \pm 8.3	81.9%	77.7% \pm 6.5	88.4% \pm 1.7
polecat	13.8%	31.2% \pm 1.5	33.5% \pm 2.8	17.7%	15.1% \pm 6.0	11.2% \pm 9.1
waffle iron	36.0%	35.5% \pm 3.9	49.4% \pm 6.8	81.2%	65.2% \pm 11.4	70.5% \pm 8.0
whippet	63.6%	22.1% \pm 2.4	44.5% \pm 11.1	51.0%	63.4% \pm 9.0	51.5% \pm 2.5
digital clock	95.3%	96.0% \pm 0.2	96.5% \pm 0.7	99.4%	99.6% \pm 0.2	99.8% \pm 0.1
colobus	3.5%	3.9% \pm 2.1	2.5% \pm 0.7	16.8%	0.5% \pm 0.1	4.1% \pm 2.9
slug	51.1%	45.1% \pm 4.7	50.7% \pm 3.5	73.8%	68.1% \pm 6.4	72.5% \pm 6.3
butcher shop	78.9%	67.9% \pm 6.3	83.5% \pm 3.3	92.2%	88.9% \pm 2.5	91.6% \pm 3.9
bluetick	46.2%	48.0% \pm 3.9	65.1% \pm 7.4	61.3%	79.2% \pm 1.9	82.0% \pm 4.2

Table 11. Success rate of targeted universal frames for each of the 10 randomly chosen target classes.

model	k	success rate (%)	successful points		all points	
			avg. queries	med. queries	avg. queries	med. queries
VGG	50	97.4 ± 0.42	497 ± 28	80 ± 4	745 ± 43	86 ± 5
	100	99.8 ± 0.14	320 ± 20	42 ± 3	335 ± 17	43 ± 3
	150	100.0 ± 0.00	193 ± 16	26 ± 2	193 ± 16	26 ± 2
ResNet	50	94.6 ± 0.70	686 ± 47	135 ± 6	1187 ± 48	166 ± 11
	100	99.7 ± 0.15	544 ± 36	73 ± 5	571 ± 26	74 ± 5
	150	100.0 ± 0.00	365 ± 19	49 ± 3	365 ± 19	49 ± 3

Table 12. Mean and standard deviation of the success rate and query efficiency of untargeted l_0 -RS repeated with 10 different random seeds. The success rate and query efficiency are very stable over random seeds.

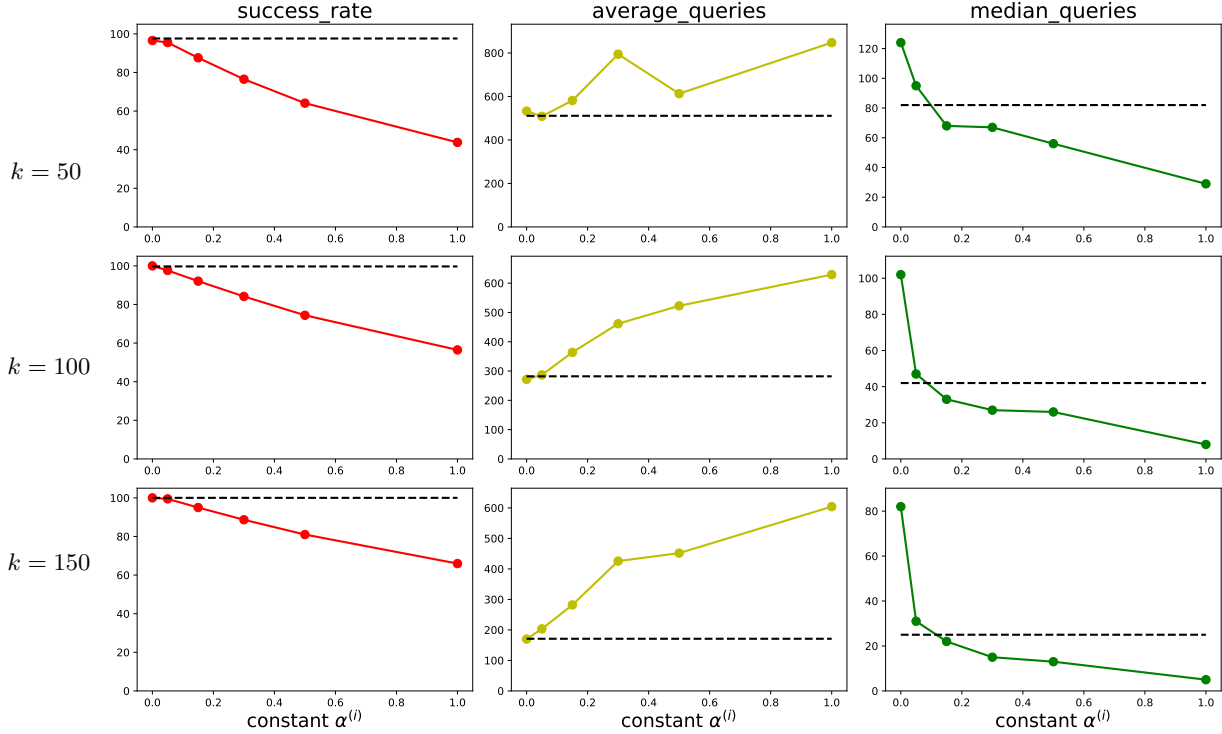


Figure 12. Performance of untargeted l_0 -RS on VGG when using a constant schedule for $\alpha^{(i)}$, that is the size of $|A| = |B| = c \cdot k$ (see Sec. 4) at every iteration, or equivalently $\alpha^{(i)} = c$ for every $i = 1, \dots, N$. The dashed line is the reference of the results achieved with the piecewise constant schedule to decay $\alpha^{(i)}$. While constantly small updates lead to good success rate, the median number of queries used increases notably, especially with larger sparsity levels k .

attack	init.	single channel	VGG			ResNet		
			succ. rate	mean queries	med. queries	succ. rate	mean queries	med. queries
Sparse-RS + SH [2]	-	-	82.6%	2479	514	75.3%	3290	549
Sparse-RS + SA [4]	stripes	no	85.6% ± 1.1	2367 ± 83	533 ± 40	78.5% ± 1.0	2877 ± 64	458 ± 43
	stripes	yes	85.7% ± 1.4	2359 ± 89	533 ± 40	79.1% ± 1.1	2861 ± 58	458 ± 43
Patch-RS	squares	no	87.1% ± 0.9	2174 ± 50	429 ± 22	78.9% ± 1.3	2820 ± 91	438 ± 68
	squares	yes	87.8% ± 0.7	2160 ± 44	429 ± 22	79.5% ± 1.4	2808 ± 89	438 ± 68

Table 13. Ablation study on the effect of initialization and single-channel updates for untargeted image-specific adversarial patches (size 20×20 pixels) within our proposed framework. We highlight in grey our modified schemes that lead to a higher success rate and query efficiency. Note that the single-channel updates come later in the optimization process when 50% success rate is reached, and thus they do not influence the median. We also report the results of Sparse-RS + SH for reference.

<i>ratio</i> <i>location : patch</i>	<i>attack</i>	VGG			ResNet		
		<i>succ. rate</i>	<i>mean queries</i>	<i>med. queries</i>	<i>succ. rate</i>	<i>mean queries</i>	<i>med. queries</i>
9:1	Sparse-RS + SH [2]	74.9%	3897	1331	68.0%	4038	1121
	Sparse-RS + SA [4]	71.4% \pm 0.9	3927 \pm 104	1361 \pm 224	68.7% \pm 1.0	3931 \pm 76	789 \pm 65
	Patch-RS	76.8% \pm 0.8	3414 \pm 48	779 \pm 69	72.0% \pm 0.8	3655 \pm 57	731 \pm 97
4:1	Sparse-RS + SH [2]	77.1%	3332	781	72.9%	3639	701
	Sparse-RS + SA [4]	77.7% \pm 1.2	3236 \pm 106	735 \pm 41	73.6% \pm 0.6	3408 \pm 35	548 \pm 65
	Patch-RS	82.4% \pm 0.8	2816 \pm 28	485 \pm 74	75.3% \pm 0.5	3248 \pm 51	443 \pm 41
1:1	Sparse-RS + SH [2]	82.9%	2718	500	75.3%	3168	451
	Sparse-RS + SA [4]	84.6% \pm 1.2	2485 \pm 92	504 \pm 20	78.2% \pm 0.7	2943 \pm 142	389 \pm 46
	Patch-RS	86.8% \pm 0.8	2301 \pm 61	352 \pm 28	79.6% \pm 1.1	2764 \pm 86	316 \pm 10
1:4	Sparse-RS + SH [2]	82.6%	2479	514	75.3%	3290	549
	Sparse-RS + SA [4]	85.6% \pm 1.1	2367 \pm 83	533 \pm 40	78.5% \pm 1.0	2877 \pm 64	458 \pm 43
	Patch-RS	87.8% \pm 0.7	2160 \pm 44	429 \pm 22	79.5% \pm 1.4	2808 \pm 89	438 \pm 68
1:9	Sparse-RS + SH [2]	80.7%	2719	564	72.2%	3451	843
	Sparse-RS + SA [4]	85.9% \pm 0.8	2419 \pm 60	542 \pm 34	77.6% \pm 0.8	3000 \pm 92	617 \pm 41
	Patch-RS	87.5% \pm 1.6	2261 \pm 44	542 \pm 39	78.4% \pm 0.6	2961 \pm 34	533 \pm 54

Table 14. Performance of different attacks for untargeted image-specific adversarial patches of size 20×20 varying the ratio between updates of the location and of the patch. We use 1:4 ratio in our framework which is the best choice for Sparse-RS + SA and Patch-RS (for Sparse-RS + SH 1:1 would work equally well). Note that our novel attack Patch-RS outperforms the competitors consistently in terms of the success rate and query efficiency across all choices of the ratio of the location and patch updates. For random search based methods, we repeat the attack with 5 random seeds.